

Stochastic Gradient MCMC for Nonlinear State Space Models

Christopher Aicher¹, Srshti Putcha², Christopher Nemeth³, Paul Fearnhead³, and Emily B. Fox^{1,4}

¹Department of Statistics, University of Washington, Seattle, WA

²STOR-i Centre for Doctoral Training, Lancaster University, Lancaster, UK

³Department of Mathematics and Statistics, Lancaster University, Lancaster, UK

⁴Paul G. Allen School of Computer Science and Engineering, University of Washington, Seattle, WA

Abstract

State space models (SSMs) provide a flexible framework for modeling complex time series via a latent stochastic process. Inference for nonlinear, non-Gaussian SSMs is often tackled with particle methods that do not scale well to long time series. The challenge is two-fold: not only do computations scale linearly with time, as in the linear case, but particle filters additionally suffer from increasing particle degeneracy with longer series. Stochastic gradient MCMC methods have been developed to scale Bayesian inference for finite-state hidden Markov models and linear SSMs using buffered stochastic gradient estimates to account for temporal dependencies. We extend these stochastic gradient estimators to nonlinear SSMs using particle methods. We present error bounds that account for both buffering error and particle error in the case of nonlinear SSMs that are log-concave in the latent process. We evaluate our proposed particle buffered stochastic gradient using stochastic gradient MCMC for inference on both long sequential synthetic and minute-resolution financial returns data, demonstrating the importance of this class of methods.

1 Introduction

Nonlinear *state space models* (SSMs) are widely used in many scientific domains for modeling time series. For example, nonlinear SSMs can be applied in engineering (e.g. target tracking, Gordon et al. 1993), in epidemiology (e.g. compartmental disease models, Dukic et al. 2012), and to financial time series (e.g. stochastic volatility models, Shephard 2005). To capture complex dynamical structure, nonlinear SSMs augment the observed time series with a latent state sequence, inducing a Markov chain dependence structure. Parameter inference for nonlinear SSMs requires us to handle this latent state sequence. This is typically achieved using *particle filtering*

methods.

Particle filtering algorithms are a set of flexible Monte Carlo simulation-based methods, which use a set of samples, also known as *particles*, to approximate the posterior distribution over the latent states. Unfortunately, inference in nonlinear SSMs does not scale well to long sequences: (i) the cost of each update requires full passes through the data that scales linearly with the length of the sequence, and (ii) the number of particles (and hence the computation per data point) required to control the bias of the particle filter scales linearly with the length of the sequence (Kantas et al., 2015).

Stochastic gradient Markov chain Monte Carlo (SG-MCMC) is a popular method for scaling Bayesian inference to large data sets, replacing full data gradients with stochastic gradient estimates based on subsets of data (Welling and Teh, 2011; Ma et al., 2015). In the context of SSMs, naive stochastic gradients are biased because subsampling breaks temporal dependencies in the data (Ma et al., 2017; Aicher et al., 2018). To correct for this, Ma et al. (2017) and Aicher et al. (2018) have developed *buffered* stochastic gradient estimators that control the bias. The latent state sequence is marginalized in a buffer around each subsequence, which reduces the effect that breaking dependencies has on the estimate of the gradient. However, the work so far has been limited to SSMs where analytic marginalization is possible (e.g. finite-state HMMs and linear dynamical systems).

In this work, we propose *particle buffered* gradient estimators that generalize the buffered gradient estimators to nonlinear SSMs. Although straightforward in concept, a number of unique challenges arise in this setting. First, we show how buffering in nonlinear SSMs can be approximated with a modified particle filter. In addition to the normal speedup gains from using a subsequence over a batch, our method also reduces the number of particles required to control the variance of the particle filter. Second, we provide an error analysis of our proposed

estimators by decomposing the error into subsequence error, buffering error, and particle filter error and analyze how this error propagates to estimating posterior means with SGMC. Third, we extend the buffering error bounds of Aicher et al. (2018) to nonlinear SSMs with log-concave likelihoods and show that buffer error decays geometrically in buffer size, ensuring that a small buffer size can be used in practice.

This paper is organized as follows. First, we review background on particle filtering in nonlinear SSMs and SGMC for analytic SSMs in Section 2. We then present our particle buffered stochastic gradient estimator in Section 3 and present the error analysis in Section 4. Finally, we test our estimator for nonlinear SSMs on both synthetic and EUR-USD exchange rate data in Section 5.

2 Background

2.1 Nonlinear State Space Models for Time Series

State space models are a class of discrete-time bivariate stochastic processes consisting of a latent state process $X = \{X_t \in \mathbb{R}^{d_x}\}_{t=1}^T$ and a second observed process, $Y = \{Y_t \in \mathbb{R}^{d_y}\}_{t=1}^T$. The evolution of the state variables is typically assumed to be a time-homogeneous Markov process, such that the latent state at time t , X_t , is determined only by the latent state at time $t-1$, X_{t-1} . The observed states are conditionally independent given the latent states. Given the prior $X_0 \sim \nu(x_0|\theta)$ and parameters $\theta \in \Theta$, the generative model for X, Y is thus

$$\begin{aligned} X_t | (X_{t-1} = x_{t-1}, \theta) &\sim p(x_t | x_{t-1}, \theta), \\ Y_t | (X_t = x_t, \theta) &\sim p(y_t | x_t, \theta), \end{aligned} \quad (1)$$

where we call $p(x_t | x_{t-1}, \theta)$ the *transition density* and $p(y_t | x_t, \theta)$ the *emission density*.

Examples of nonlinear SSMs include the *stochastic volatility model* (SVM) (Shephard, 2005) and the *generalized autoregressive conditional heteroskedasticity* (GARCH) model (Bollerslev, 1986). For a review of applications of state space modeling, see Langrock (2011).

For an arbitrary sequence $\{z_i\}$, we use $z_{i:j}$ to denote the sequence $(z_i, z_{i+1}, \dots, z_j)$. To infer the model parameters θ , a quantity of interest is the *score function*, gradient of the marginal loglikelihood, $\nabla_\theta \log p(y_{1:T}|\theta)$. Using the score function, the loglikelihood can for instance be maximized iteratively via a (batch) *gradient ascent* algorithm (Robbins and Monro, 1951), given the observations, $y_{1:T}$.

If the latent state posterior $p(x_{1:T}|y_{1:T}, \theta)$ can be expressed analytically, we can calculate the score using

Fisher's identity (Cappé et al., 2005),

$$\begin{aligned} \nabla_\theta \log p(y_{1:T} | \theta) &= \mathbb{E}_{X|Y,\theta} [\nabla_\theta \log p(X_{1:T}, y_{1:T} | \theta)] \\ &= \sum_{t=1}^T \mathbb{E}_{X|Y,\theta} [\nabla_\theta \log p(X_t, y_t | x_{t-1}, \theta)]. \end{aligned} \quad (2)$$

However, if the latent state posterior, $p(x_{1:T}|y_{1:T}, \theta)$, is not available in closed-form, we can approximate the expectations of the latent state posterior. One popular approach is via *particle filtering* methods.

2.1.1 Particle Filtering and Smoothing

Particle filtering algorithms (see e.g. Doucet and Johansen, 2009; Fearnhead and Künsch, 2018) can be used to create an empirical approximation of the expectation of a function $H(X_{1:T})$ with respect to the posterior density, $p(x_{1:T}|y_{1:T}, \theta)$. This is done by generating a collection of N random samples or *particles*, $\{x_t^{(i)}\}_{i=1}^N$ and calculating their associated importance weights, $\{w_t^{(i)}\}_{i=1}^N$, recursively over time. We update the particles and weights with *sequential importance resampling* (SIR) (Doucet and Johansen, 2009) in the following manner.

- (i) *Resample* auxiliary ancestor indices $\{a_1, \dots, a_N\}$ with probabilities proportional to the importance weights, i.e. $a_i \sim \text{Categorical}(w_{t-1}^{(i)})$.
- (ii) *Propagate* particles $x_t^{(i)} \sim q(\cdot | x_{t-1}^{(a_i)}, y_t, \theta)$, using a proposal distribution $q(\cdot | \cdot)$.
- (iii) *Update* and normalize the weight of each particle,

$$w_t^{(i)} \propto \frac{p(y_t | x_t^{(i)}, \theta) p(x_t^{(i)} | x_{t-1}^{(a_i)}, \theta)}{q(x_t^{(i)} | x_{t-1}^{(a_i)}, y_t, \theta)}, \quad \sum_i w_t^{(i)} = 1. \quad (3)$$

The auxiliary variables, $\{a_i\}_{i=1}^N$, represent the indices of the *ancestors* of the particles, $\{x_t^{(i)}\}_{i=1}^N$, sampled at time t . The introduction of ancestor indices allows us to keep track of the lineage of particles over time (Andrieu et al., 2010). The *multinomial resampling* scheme given in (i) describes the procedure by which *offspring* particles are produced.

Resampling at each iteration is used to mitigate against the problem of *weight degeneracy*. This phenomenon occurs when the variance of the importance weights grows, causing more and more particles to have negligible weight. Aside from the multinomial resampling scheme described above, there are various other

resampling schemes outlined in the particle filtering literature, such as stratified sampling (Kitagawa, 1996) and residual sampling (Liu and Chen, 1998).

If the proposal density $q(x_t|x_{t-1}, y_t, \theta)$ is the transition density $p(x_t|x_{t-1}, \theta)$, SIR is also known as the *bootstrap particle filter* (Gordon et al., 1993). By using the transition density for proposals, the importance weight recursion in Eq. (3) simplifies to $w_t^{(i)} \propto p(y_t|x_t^{(i)}, \theta)$.

When our target function decomposes into a pairwise sum $H(x_{1:T}) = \sum_{t=1}^T h_t(x_t, x_{t-1})$ – such as for Fisher’s identity $h_t(x_t, x_{t-1}) = \nabla_\theta \log p(y_t, x_t | x_{t-1}, \theta)$ – then we only need to keep track of the partial sum $H_t = \sum_{s=1}^t h_s(x_s, x_{s-1})$ rather than the full list of $x_{1:t}$ during SIR. The complete particle filtering scheme is detailed in Algorithm 1.

Algorithm 1 Particle Filter

- 1: **Input:** number of particles, N , pairwise statistics, $h_{1:T}$, observations $y_{1:T}$, proposal density q .
- 2: Draw $x_0^{(i)} \sim \nu(x_0|\theta)$, set $w_0^{(i)} = \frac{1}{N}$, and $H_0^{(i)} = 0 \forall i$.
- 3: **for** $t = 1, \dots, T$ **do**
- 4: Resample ancestor indices $\{a_1, \dots, a_N\}$.
- 5: Propagate particles $x_t^{(i)} \sim q(\cdot|x_{t-1}^{(a_i)}, y_t, \theta)$.
- 6: Update each $w_t^{(i)}$ according to Eq. (3).
- 7: Update statistics $H_t^{(i)} = H_{t-1}^{(a_i)} + h_t(x_t^{(i)}, x_{t-1}^{(a_i)})$.
- 8: **end for**
- 9: Return $H = \sum_{i=1}^N w_T^{(i)} H_T^{(i)}$.

A key challenge for particle filters is handling large T . Not only do long sequences require $\mathcal{O}(T)$ computation, but particle filters require a large number of particles, N , to avoid *particle degeneracy*: the use of resampling in the particle filter causes path-dependence over time, depleting the number of distinct particles available overall. For Algorithm 1, the variance in H scales as $\mathcal{O}(T^2/N)$ (Poyiadjis et al., 2011). Therefore to maintain a constant variance, the number of particles would need to increase quadratically with T , which is computationally infeasible for long sequences. Poyiadjis et al. (2011); Nemeth et al. (2016) and Olsson and Westerborn (2017) propose alternatives to Step 7 of Algorithm 1 that trade additional computation or bias to decrease the variance in H to $\mathcal{O}(T/N)$. Fixed-lag particle smoothers provide another approach to avoid particle degeneracy, where sample paths are not updated after a fixed lag (Kitagawa and Sato, 2001; Dahlin et al., 2015). All of these methods perform a full pass over the data $y_{1:T}$, which requires $\mathcal{O}(T)$ computation.

2.2 Stochastic Gradient MCMC

One popular method to conduct scalable Bayesian inference for large data sets is *stochastic gradient* Markov chain Monte Carlo (SGMCMC). Given a prior $p(\theta)$, to draw a sample θ from the posterior $p(\theta|y) \propto p(y|\theta)p(\theta)$, gradient-based MCMC methods simulate a stochastic differential equation (SDE) based on the gradient of the loglikelihood $g_\theta = \nabla_\theta \log p(y|\theta)$, such that the posterior is the stationary distribution of the SDE. SGMCMC methods replace the full-data gradients with stochastic gradients, \hat{g}_θ , using subsamples of the data to avoid costly computation.

The most common method of the SGMCMC family is the *stochastic gradient Langevin dynamics* (SGLD) algorithm (Welling and Teh, 2011; Nemeth and Fearnhead, 2019):

$$\theta^{(k+1)} \leftarrow \theta^{(k)} + \epsilon^{(k)} \cdot (\hat{g}_\theta + \nabla \log p(\theta)) + \mathcal{N}(0, 2\epsilon^{(k)}), \quad (4)$$

where $\epsilon^{(k)}$ is the stepsize. When \hat{g}_θ is unbiased and with an appropriate decreasing stepsize, the distribution of $\theta^{(k)}$ asymptotically converges to the posterior distribution (Teh et al., 2016). Dalalyan and Karagulyan (2017) provide non-asymptotic bounds on the Wasserstein distance between the posterior and the output of SGLD after K steps for fixed $\epsilon^{(k)} = \epsilon$ and possibly biased \hat{g}_θ .

Many extensions of SGLD exist in the literature, including using control variates to reduce the variance of \hat{g}_θ (Baker et al., 2018; Nagapetyan et al., 2017; Chatterji et al., 2018) and augmented dynamics to improve mixing (Ma et al., 2015) such as stochastic gradient Hamiltonian Monte Carlo (Chen et al., 2014), stochastic gradient Nosé-Hoover thermostat (Ding et al., 2014), and stochastic gradient Riemannian Langevin dynamics (Girolami and Calderhead, 2011; Patterson and Teh, 2013).

2.2.1 Stochastic Gradients for SSMs

An additional challenge when applying SGMCMC to SSMs is handling the temporal dependence between observations. Based on a subset \mathcal{S} of size S , an unbiased stochastic gradient estimate of Eq. (2) is

$$\sum_{t \in \mathcal{S}} \Pr(t \in \mathcal{S})^{-1} \cdot \mathbb{E}_{X|y_{1:T}, \theta} [\nabla_\theta \log p(X_t, y_t | X_{t-1}, \theta)]. \quad (5)$$

Although Eq. (5) is a sum over S terms, it requires taking expectations with respect to $p(x|y_{1:T}, \theta)$, which requires processing the full sequence $y_{1:T}$. One approach to reduce computation is to randomly sample \mathcal{S} as a contiguous subsequence $\mathcal{S} = \{s+1, \dots, s+S\}$ and

approximate Eq. (5) using only y_S

$$\sum_{t \in \mathcal{S}} \Pr(t \in \mathcal{S})^{-1} \cdot \mathbb{E}_{X|y_S, \theta} [\nabla_\theta \log p(X_t, y_t | X_{t-1}, \theta)]. \quad (6)$$

However, Eq. (6) is *biased* because the expectation over the latent states x_S is conditioned only on y_S rather than $y_{1:T}$.

To control the bias in stochastic gradients while also avoiding accessing the full sequence, previous work on SGMCMC for SSMs proposed *buffered* stochastic gradients (Ma et al., 2017; Aicher et al., 2018).

$$\hat{g}_\theta(S, B) = \sum_{t \in \mathcal{S}} \frac{\mathbb{E}_{X|y_{S^*}, \theta} [\nabla_\theta \log p(X_t, y_t | X_{t-1}, \theta)]}{\Pr(t \in \mathcal{S})}, \quad (7)$$

where $\mathcal{S}^* = \{s+1-B, \dots, s+S+B\}$ is the *buffered* subsequence such that $\mathcal{S} \subseteq \mathcal{S}^* \subseteq \{1, \dots, T\}$ (see Figure 1). Note Eq. (5) is $\hat{g}(S, T)$ and Eq. (6) is $\hat{g}(S, 0)$. As B increases from 0 to T , the estimator $\hat{g}_\theta(S, B)$ trades computation for reduced bias. In particular, when the

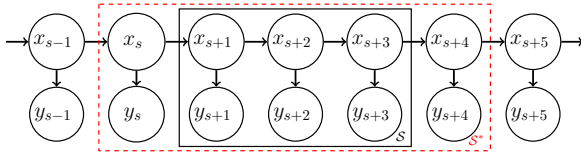


Figure 1: Graphical model of \mathcal{S}^* with $S = 3$ and $B = 1$.

model and gradient both satisfy a Lipschitz property, the error decays geometrically in buffer size B , see Theorem 4.1 of Aicher et al. (2018). Specifically, for all \mathcal{S}

$$\|\hat{g}_\theta(S, B) - \hat{g}_\theta(S, T)\|_2 = \mathcal{O}((L_\theta)^B T / S), \quad (8)$$

where L_θ is a bound for the Lipschitz constants of the *forward and backward smoothing kernels*¹

$$\begin{aligned} \vec{\Psi}_t(x_{t+1}, x_t) &= p(x_{t+1} | x_t, y_{1:T}, \theta), \\ \bar{\Psi}_t(x_{t-1}, x_t) &= p(x_{t-1} | x_t, y_{1:T}, \theta). \end{aligned} \quad (9)$$

The bound provided in Eq. (8) ensures that only a modest buffer size B is required (e.g. $\mathcal{O}(\log \delta^{-1})$ for an accuracy of δ). Unfortunately, neither the buffered stochastic gradient $\hat{g}_\theta(S, B)$ nor the smoothing kernels $\{\vec{\Psi}_t, \bar{\Psi}_t\}$ have a closed-form for nonlinear SSMs.

3 Method

In this section, we propose a particle buffered stochastic gradient for nonlinear SSMs, by applying the particle approximations of Section 2.1 to Eq. (7).

¹We follow Aicher et al. (2018) and consider Lipschitz constants for a kernel Ψ measured in terms of the p -Wasserstein distance between distributions of x, x' and $\Psi(x), \Psi(x')$.

3.1 Buffered Stochastic Gradient Estimates for Nonlinear SSMs

Let $g_\theta^{\text{PF}}(S, B, N)$ denote the particle approximation of $\hat{g}_\theta(S, B)$ with N particles. We approximate the expectation over $p(x|y_{S^*}, \theta)$ in Eq. (7) using Algorithm 1 run over \mathcal{S}^* with prior ν_0 for X_{s+1-B} . In particular, the complete data loglikelihood, $\log p(y_S, x_S, \theta)$, in Eq. (7) decomposes into a sum of pairwise statistics

$$H = \sum_{t \in \mathcal{S}^*} h_t(x_t, x_{t-1}), \quad (10)$$

where

$$h_t(x_t, x_{t-1}) = \begin{cases} \frac{\nabla_\theta \log p(x_t, y_t | x_{t-1}, \theta)}{\Pr(t \in \mathcal{S})} & \text{if } t \in \mathcal{S}, \\ 0 & \text{otherwise.} \end{cases} \quad (11)$$

We highlight that the statistic is zero for t in the left and right buffers $\mathcal{S}^* \setminus \mathcal{S}$. Although H_t is not updated by h_t for t in $\mathcal{S}^* \setminus \mathcal{S}$, running the particle filter over the buffers is *crucial* to reduce the bias of $g_\theta^{\text{PF}}(S, B, N)$.

Note that $g_\theta^{\text{PF}}(S, B, N)$ allows us to approximate the non-analytic expectation in Eq. (7) with a modest number of particles N , by avoiding the particle degeneracy and full sequence runtime bottlenecks, as the particle filter is only run over \mathcal{S}^* , which has length $S + 2B \ll T$.

3.2 SGMCMC Algorithm

Using $g_\theta^{\text{PF}}(S, B, N)$ as our stochastic gradient estimate in SGLD, Eq. (4), gives us Algorithm 2.²

Algorithm 2 Buffered PF-SGLD

- 1: Input: data $y_{1:T}$, initial $\theta^{(0)}$, stepsize ϵ , subsequence size S , buffer size B , particle size N
- 2: **for** $k = 1, 2, \dots, K$ **do**
- 3: Sample $\mathcal{S} = \{s+1, \dots, s+S\}$
- 4: Set $\mathcal{S}^* = \{s+1-B, \dots, s+S+B\}$.
- 5: Calculate g_θ^{PF} over \mathcal{S}^* using Alg. 1 on Eq. (11).
- 6: Set $\theta^{(k+1)} \leftarrow \theta^{(k)} + \epsilon \cdot (g_\theta^{\text{PF}} + \nabla \log p(\theta)) + \mathcal{N}(0, 2\epsilon)$
- 7: **end for**
- 8: Return $\theta^{(K+1)}$

Algorithm 2 can be extended by (i) averaging over multiple sequences or varying the subsequence sampling method (Schmidt et al., 2015; Ou et al., 2018), (ii) using different particle filters such as those listed in Section 2.1.1, and (iii) using more advanced SGMCMC schemes such as those listed in Section 2.2.

²Python code for Algorithm 2 and experiments of Section 5 is available at https://github.com/aicherc/sgmcmc_ssm_code.

4 Error Analysis

In this section, we analyze the error of our particle buffered stochastic gradient g_θ^{PF} and its effect on approximating posterior means with finite sample averages using Algorithm 2. We first present error bounds for approximating posterior means using SGLD with biased gradients (Theorem 1). We then present bounds on the gradient bias and MSE of g_θ^{PF} , extending the error bounds of Aicher et al. (2018) (Theorem 2). In particular, we provide bounds for the Lipschitz constant L_θ of the smoothing kernels Eq. (9) without requiring an explicit form for the smoothing kernels (Theorem 3), allowing Eq. (8) to apply to nonlinear SSMs.

4.1 Error of Biased SGLD's Finite Sample Averages

We consider the estimation error of the posterior expected value of some test function of the parameters $\phi: \Theta \rightarrow \mathbb{R}$ using samples $\theta^{(k)}$ drawn using SGLD with a fixed step-size ϵ and stochastic gradients g_θ .

Let $\bar{\phi}$ be the posterior expected value

$$\bar{\phi} = \mathbb{E}_{p(\theta|y)}[\phi(\theta)] , \quad (12)$$

and let $\hat{\phi}_{K,\epsilon}$ be the K -sample estimator for $\bar{\phi}$

$$\hat{\phi}_{K,\epsilon} = \frac{1}{K} \sum_{k=1}^K \phi(\theta^{(k)}) . \quad (13)$$

The error of the *finite sample average* $|\hat{\phi}_{K,\epsilon} - \bar{\phi}|$ has been previously studied for SGLD with *unbiased* gradients by Vollmer et al. (2016) and Chen et al. (2015). We now present Theorem 1, which bounds the error of finite sample average of SGLD when the stochastic gradients \hat{g}_θ are potentially *biased*.

Theorem 1 (Error of Finite Sample Average). *If the gradient g_θ is smooth in θ , the test function ϕ satisfies a moment condition (described in the Appendix) and the bias and MSE of the gradient estimates \hat{g}_θ are uniformly bounded, that is,*

$$\mathbb{E} \|\hat{g}_\theta - g_\theta\| \leq \delta \text{ and } \mathbb{E} \|\hat{g}_\theta - g_\theta\|^2 \leq \sigma^2 \text{ for all } \theta , \quad (14)$$

then the bias and MSE of $\hat{\phi}_{K,\epsilon}$ satisfy

$$|\mathbb{E} \hat{\phi}_{K,\epsilon} - \bar{\phi}| = \mathcal{O} \left(\frac{1}{K\epsilon} + \epsilon + \delta \right) , \quad (15)$$

$$\mathbb{E} |\hat{\phi}_{K,\epsilon} - \bar{\phi}|^2 = \mathcal{O} \left(\frac{1}{K\epsilon} + \epsilon^2 + \frac{\sigma^2}{K} + \delta^2 + \frac{\delta}{\epsilon} + \delta\epsilon \right) . \quad (16)$$

The bias bound, Eq. (15), is a direct application of Theorem 2 in Chen et al. (2015). The MSE bound, Eq. (16), is an extension of Theorem 3 in Chen et al. (2015) when the stochastic gradient estimates \hat{g}_θ are biased (i.e. $\delta \neq 0$). The additional bias terms δ arise from keeping track of additional cross terms in $(\hat{\phi}_{K,\epsilon} - \bar{\phi})^2$. The proof of Theorem 1 is presented in the Appendix.

From Theorem 1, we see that the error bounds on $\hat{\phi}_{K,\epsilon}$ are more sensitive to the bias δ of \hat{g} than the variance σ^2 : the term involving σ^2 decays with increasing K , while terms involving δ do not decay regardless of stepsize ϵ or number of samples K . Therefore for the samples from Algorithm 2 to be useful, it is important for the bias of g_θ^{PF} to be controlled.

4.2 Gradient Bias and MSE Bounds

To apply Theorem 1 to the samples from Algorithm 2, we develop bounds on the bias δ and MSE σ^2 of our particle buffered stochastic gradients g_θ^{PF} .

Theorem 2 (Bias and MSE Bounds for g_θ^{PF}). *For fixed θ , if the model and gradient satisfy a Lipschitz condition and there is a bound on the autocorrelation, then the bias δ and MSE σ^2 of g_θ^{PF} is bounded by*

$$\delta \leq \gamma \cdot \left[C_1(L_\theta)^B + \mathcal{O} \left(\frac{S+2B}{N} \right) \right] , \quad (17)$$

$$\sigma^2 \leq 3\gamma^2 \cdot \left[C_1^2(L_\theta)^{2B} + C_2 S + \mathcal{O} \left(\frac{(S+2B)^2}{N} \right) \right] , \quad (18)$$

where $\gamma = \max_t \Pr(t \in \mathcal{S})^{-1}$ and C_1, C_2 are constants with respect to S, B, N .

From Theorem 2, we see that the bias δ Eq. (17) can be controlled by selecting large enough N and B .

We now sketch the proof of Theorem 2 and discuss its assumptions. The complete proof can be found in the Appendix.

We decompose the error between g_θ^{PF} and the full gradient g_θ through $\hat{g}_\theta(S, B)$ and $\hat{g}_\theta(S, T)$ into three error sources:

$$\begin{aligned} \|g_\theta^{\text{PF}}(S, B, N) - g_\theta\| &\leq \underbrace{\|g_\theta^{\text{PF}}(S, B, N) - \hat{g}_\theta(S, B)\|}_{\text{particle error (I)}} + \\ &\quad \underbrace{\|\hat{g}_\theta(S, B) - \hat{g}_\theta(S, T)\|}_{\text{buffering error (II)}} + \underbrace{\|\hat{g}_\theta(S, T) - g_\theta\|}_{\text{subsequence error (III)}} . \end{aligned} \quad (19)$$

(I) *Particle error*: the Monte Carlo error of the particle filter. From Kantas et al. (2015), the

asymptotic bias and MSE of a particle approximation to the sum of R test functions (using Algorithm 1) is $\mathcal{O}(R/N)$ and $\mathcal{O}(R^2/N)$ respectively. Since $g^{\text{PF}}(S, B, N)$ is a particle approximation to the sum of $R = S + 2B$ test functions (i.e., $h_t(x_t, x_{t-1})$), we have

$$\begin{aligned} \|\mathbb{E} g_{\theta}^{\text{PF}}(S, B, N) - \hat{g}_{\theta}(S, B)\| \\ = \mathcal{O}\left(\gamma \cdot \frac{S + 2B}{N}\right), \\ \mathbb{E} \|g_{\theta}^{\text{PF}}(S, B, N) - \hat{g}_{\theta}(S, B)\|^2 \\ = \mathcal{O}\left(\gamma^2 \cdot \frac{(S + 2B)^2}{N}\right). \end{aligned} \quad (20)$$

where γ is a upper bound on the sampling scale factor $\gamma = \max_t \Pr(t \in \mathcal{S})^{-1}$.

Using a more advanced particle filter, such as the PaRIS algorithm, Corollary 6 of Olsson and Westerborn (2017) gives a tighter bound for the MSE

$$\begin{aligned} \mathbb{E} \|g_{\theta}^{\text{PF}}(S, B, N) - \hat{g}_{\theta}(S, B)\|^2 \\ = \mathcal{O}\left(\gamma^2 \cdot \frac{S + 2B}{N}\right). \end{aligned}$$

However in our experiments, we found that the improved MSE of PaRIS was not worth the additional computational overhead of the PaRIS algorithm for the small subsequences we considered. $S + 2B \lesssim 100$ (see experiments in the Appendix).

- (II) *Buffering error*: error in approximating the latent state posterior $p(x_{1:T}|y_{1:T})$ with $p(x_{1:T}|y_{\mathcal{S}^*})$. If the smoothing kernels $\{\vec{\Psi}_t, \tilde{\Psi}_t\}$ are contractions for all t (i.e. $L_{\theta} < 1$), then according to Eq. (8), the error in this term is proportional to $\gamma(L_{\theta})^B$. In Section 4.3, we show sufficient conditions for $L_{\theta} < 1$.
- (III) *Subsequence error*: the error in approximating Fisher's identity with a stochastic subsequence. The error in this term depends on the subsequence size S and how subsequences are sampled. Because we sample random *contiguous* subsequences of size S , the MSE scales $\mathcal{O}(\gamma^2 S \frac{1+\rho}{1-\rho})$, where ρ is a bound on the autocorrelation between terms (see the Appendix for details).

Combining these error bounds gives us Theorem 2.

We present examples of the asymptotic bias and MSE bounds given by Theorem 2 for four different gradient estimators in Table 1. The four gradient estimators are: (i) naive stochastic subsequence (without

buffering) $g^{\text{PF}}(S, 0, N)$ (ii) buffered stochastic subsequence $g^{\text{PF}}(S, B, N)$, (iii) fully buffered subsequence $g^{\text{PF}}(S, T, N)$, and (iv) full sequence $g^{\text{PF}}(T, T, N)$. For simplicity, we assume the subsequences \mathcal{S} are sampled from a *strict* partition of $1 : T$ such that $\gamma = T/S$ and assume B is on the same order as S (i.e. B is $\mathcal{O}(S)$).

From Table 1, we see that without buffering, the naive stochastic gradient has a T/S term in the bias bound δ . The fully buffered subsequence and full sequence gradients remove the buffering error entirely at the cost of $\mathcal{O}(TN)$ computation (instead of $\mathcal{O}(SN)$). Instead, our proposed buffered stochastic gradient controls the bias, with the geometrically decaying factor $(L_{\theta})^B$, using only $\mathcal{O}(SN)$ computation.

4.3 Buffering Error Bound for Nonlinear SSMS

To obtain a bound for the buffering error term (II), we require the Lipschitz constant L_{θ} of smoothing kernels $\{\vec{\Psi}_t, \tilde{\Psi}_t\}$ to be less than 1. Typically the smoothing kernels $\vec{\Psi}_t, \tilde{\Psi}_t$ are not available in closed-form for nonlinear SSMS and therefore directly bounding the Lipschitz constant is difficult. However, we now show that when the model's transition and emission densities are *log-concave* in x_t, x_{t-1} , we can bound the Lipschitz constant of $\vec{\Psi}_t, \tilde{\Psi}_t$ in terms of the Lipschitz constant of either the *prior kernels* $\vec{\Psi}_t^{(0)}, \tilde{\Psi}_t^{(0)}$, or the *filtered kernels* $\vec{\Psi}_t^{(1)}, \tilde{\Psi}_t^{(1)}$

$$\begin{aligned} \vec{\Psi}_t^{(0)} &:= p(x_t | x_{t-1}, \theta), & \vec{\Psi}_t^{(1)} &:= p(x_t | x_{t-1}, y_t, \theta), \\ \tilde{\Psi}_t^{(0)} &:= p(x_t | x_{t+1}, \theta), & \tilde{\Psi}_t^{(1)} &:= p(x_t | x_{t+1}, y_t, \theta), \end{aligned} \quad (21)$$

Unlike the smoothing kernels, the prior kernels are defined by the model and are therefore usually available. If the filtered kernels are available, then they can be used to obtain even tighter bounds.

Theorem 3 (Lipschitz Kernel Bound). *Assume the prior for x_0 is log-concave in x . If the transition density $p(x_t | x_{t-1}, \theta)$ is log-concave in (x_t, x_{t-1}) and the emission density $p(y_t | x_t)$ is log-concave in x_t , then*

$$\|\vec{\Psi}_t\|_{Lip} \leq \|\vec{\Psi}_t^{(1)}\|_{Lip} \leq \|\vec{\Psi}_t^{(0)}\|_{Lip} \quad (22)$$

$$\|\tilde{\Psi}_t\|_{Lip} \leq \|\tilde{\Psi}_t^{(1)}\|_{Lip} \leq \|\tilde{\Psi}_t^{(0)}\|_{Lip}. \quad (23)$$

Therefore

$$\begin{aligned} L_{\theta} &= \max_t \{\|\vec{\Psi}_t\|_{Lip}, \|\tilde{\Psi}_t\|_{Lip}\} \\ &\leq \max_t \{\|\vec{\Psi}_t^{(1)}\|_{Lip}, \|\tilde{\Psi}_t^{(1)}\|_{Lip}\} \\ &\leq \max_t \{\|\vec{\Psi}_t^{(0)}\|_{Lip}, \|\tilde{\Psi}_t^{(0)}\|_{Lip}\} \end{aligned} \quad (24)$$

Table 1: Asymptotic bias, MSE, and computation cost for four different gradient estimators.

Gradient	(S, B, N)	Bias δ	MSE σ^2	Compute
Naive Stochastic Subsequence	$(S, 0, N)$	$\mathcal{O}(T/N + T/S)$	$\mathcal{O}(T^2/N + T^2/S)$	$\mathcal{O}(SN)$
Buffered Stochastic Subsequence	(S, B, N)	$\mathcal{O}(T/N + (L_\theta)^B \cdot T/S)$	$\mathcal{O}(T^2/N + T^2/S)$	$\mathcal{O}(SN)$
Fully Buffered Subsequence	(S, T, N)	$\mathcal{O}(T/N)$	$\mathcal{O}(T^2/N + T^2/S)$	$\mathcal{O}(TN)$
Full Sequence	(T, T, N)	$\mathcal{O}(T/N)$	$\mathcal{O}(T^2/N)$	$\mathcal{O}(TN)$

This theorem lets us bound L_θ with the Lipschitz constant of either the prior kernels or filtered kernels. The proof of Theorem 3 is provided in the Appendix and uses Caffarelli’s log-concave perturbation theorem (Villani, 2008; Colombo et al., 2015). Examples of SSMs that are log-concave include the linear Gaussian SSM, the stochastic volatility model, or any linear SSM with log-concave transition and emission distributions. Examples of SSMs that are not log-concave include the GARCH model or any linear SSM with a transition or emission distribution that is not log-concave (e.g. Student’s t).

Theorem 3 let us calculate analytic bounds on L_θ for the buffering error of Theorem 2. We provide explicit bounds for L_θ for the linear Gaussian SSM and stochastic volatility model in Section 5.1 with proofs in the Appendix.

5 Experiments

We first empirically test the bias of our particle buffered gradient estimator g_θ^{PF} on synthetic data for fixed θ . We then evaluate the performance of our proposed SGLD algorithm (Algorithm 2) on both real and synthetic data.

5.1 Models

For our experiments, we consider three models: (i) linear Gaussian SSM (LGSSM), a case where analytic buffering is possible, to assess the impact of the particle filter; (ii) the SVM, where the emissions are non-Gaussian; and (iii) a GARCH model, where the latent transitions are nonlinear.

5.1.1 Linear Gaussian SSM

The *linear Gaussian SSM* (LGSSM) is

$$\begin{aligned} X_t | (X_{t-1} = x_{t-1}, \theta) &\sim \mathcal{N}(x_t | \phi x_{t-1}, \sigma^2), \\ Y_t | (X_t = x_t, \theta) &\sim \mathcal{N}(y_t | x_t, \tau^2), \end{aligned} \quad (25)$$

with $X_0 \sim \mathcal{N}(x_0 | 0, \frac{\phi^2}{1-\sigma^2})$ and parameters $\theta = (\phi, \sigma, \tau)$.

The transition and emission distributions are both Gaussian and log-concave in x , so Theorem 3 applies.

In the Appendix, we show that the filtered kernels of the LGSSM are bounded with the Lipschitz constant $L_\theta = |\phi| \cdot \sigma^2 / (\sigma^2 + \tau^2)$. Thus, the buffering error decays geometrically with increasing buffer size B when $|\phi| < (1 + \frac{\tau^2}{\sigma^2})$. This linear model serves as a useful baseline since the various terms in Eq. (19) can be calculated analytically.

5.1.2 Stochastic Volatility Model

The *stochastic volatility model* (SVM) is

$$\begin{aligned} X_t | (X_{t-1} = x_{t-1}, \theta) &\sim \mathcal{N}(x_t | \phi x_{t-1}, \sigma^2), \\ Y_t | (X_t = x_t, \theta) &\sim \mathcal{N}(y_t | 0, \exp(x_t) \tau^2), \end{aligned} \quad (26)$$

with parameters $\theta = (\phi, \sigma, \tau)$.

For the SVM, the transition and emission distributions are log-concave in x , allowing Theorem 3 to apply. In the Appendix, we show that the prior kernels $\{\tilde{\Psi}_t^{(0)}, \tilde{\Psi}_t^{(0)}\}$ of the SVM are bounded with the Lipschitz constant $L_\theta = |\phi|$. Thus, the buffering error decays geometrically with increasing buffer size B when $|\phi| < 1$.

5.1.3 GARCH Model

We finally consider a GARCH(1,1) model (with noise)

$$\begin{aligned} X_t | (X_{t-1} = x_{t-1}, \sigma_t^2, \theta) &\sim \mathcal{N}(x_t | 0, \sigma_t^2), \\ \sigma_t^2 | (x_{t-1}, \sigma_{t-1}^2, \theta) &= \alpha + \beta x_{t-1}^2 + \gamma \sigma_{t-1}^2, \\ Y_t | (X_t = x_t, \theta) &\sim \mathcal{N}(y_t | x_t, \tau^2), \end{aligned} \quad (27)$$

with parameters $\theta = (\alpha, \beta, \gamma, \tau)$. Unlike the LGSSM and SVM, the noise between X_t and X_{t-1} is multiplicative in X_{t-1} rather than additive. This model is *not* log-concave and therefore our theory (Theorem 3) does not hold. However, we see empirically that buffering can help reduce the gradient error for the GARCH in the experiments below and in the Appendix.

5.2 Stochastic Gradient Bias

We compare the error of stochastic gradient estimates using a buffered subsequence with $S = 16$, while varying B and N on synthetic data from each model. We generated

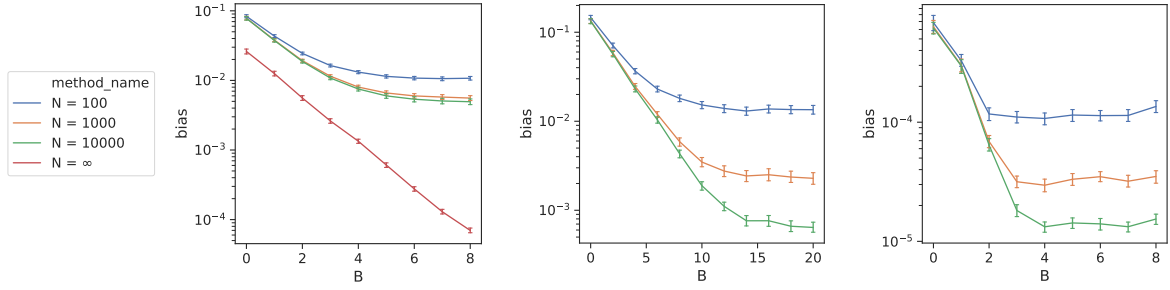


Figure 2: Stochastic gradient bias varying buffer size B for $S = 16$ for different values of N . (left) LGSSM ϕ , (middle) SVM ϕ , (right) GARCH β . Error bars are 95% CI over 1000 replications.

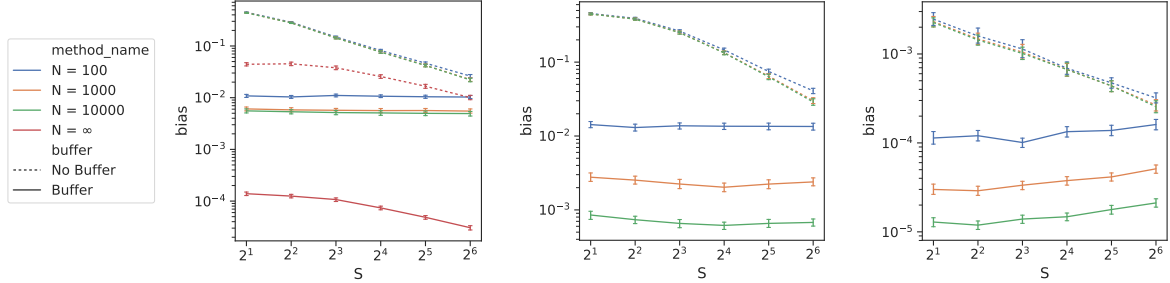


Figure 3: Stochastic gradient bias varying subsequence size S for No Buffer ($B = 0$) and Buffer ($B > 0$) for different values of N . (left) LGSSM ϕ , (middle) SVM ϕ , (right) GARCH β . The buffer size $B = 8$ for LGSSM and GARCH and $B = 16$ for the SVM. Error bars are 95% CI over 1000 replications.

synthetic data of length $T = 256$ using $(\phi = 0.9, \sigma = 0.7, \tau = 1.0)$ for the LGSSM, $(\phi = 0.9, \sigma = 0.5, \tau = 0.5)$ for the SVM, and $(\alpha = 0.1, \beta = 0.8, \gamma = 0.05, \tau = 0.3)$ for the GARCH model.

Figures 2-4 display the bias of our particle buffered stochastic gradient $g_\theta^{\text{PF}}(S, B, N)$ and g_θ averaged over 1000 replications. We evaluate the gradients at θ equal to the data generating parameters. We vary the buffer size $B \in [0, 16]$, the subsequence size $S \in [1, T]$ and the number of samples $N \in \{100, 1000, 10000\}$. For the LGSSM, we also consider $N = \infty$, by calculating $g_\theta^{\text{PF}}(S, B, \infty)$ using the Kalman filter, which is tractable in the linear setting. We calculate g_θ using the Kalman filter for the LGSSM, and use $g_\theta \approx g_\theta^{\text{PF}}(T, 0, 10^7)$ for the SVM and the GARCH model, assuming that $N = 10^7$ particles is sufficient for an accurate approximation in these 1-dimensional settings.

Figure 2 shows the bias as we vary the buffer size B for different N and $S = 16$. From Figure 2, we see the trade-off between the buffering error (II) and the particle error (III) in the bias bound, Eq. (17) of Theorem 2. For all N , when B is small, the buffering error (II) dominates, and therefore the MSE decays exponentially as B increases. However for $N < \infty$, the particle error (III) dominates for larger values of B . In fact, the bias slightly increases due to particle degeneracy, as $|S^*| = S + 2B$ increases

with B . For $N = \infty$ in the LGSSM case, we see that the bias continues to decreases exponentially with large B as there is no particle filter error when using the Kalman filter.

Figure 3 shows the bias as we vary the subsequence size S for different N and with and without buffering. We see that buffering helps regardless of subsequence size (as the bias for all buffered methods are lower than the no buffer methods for all $S \in [2, 64]$). We also see that increasing S can increase the bias for fixed N (when buffering) as the particle error (III) dominates.

Figure 4 shows the bias as we vary the number of particles N for the four different methods correspond to Table 1. In the top row, we compare the bias against N and in the bottom row, we compare the bias against the runtime required to calculate g_θ^{PF} . We see that the method without buffering (orange) is significantly biased regardless of N , whereas buffering with moderate B (blue), buffering with large $B = T$ (red), and using the full sequence (green) have similar (lower) bias as we increase N . However the runtime plots show that buffering with moderate B takes significantly less time.

In summary, Figures 2-4 show that buffering cannot be ignored in these three example models: there is high bias for $B = 0$. In general, buffering has diminishing returns when B is excessively large relative to N .

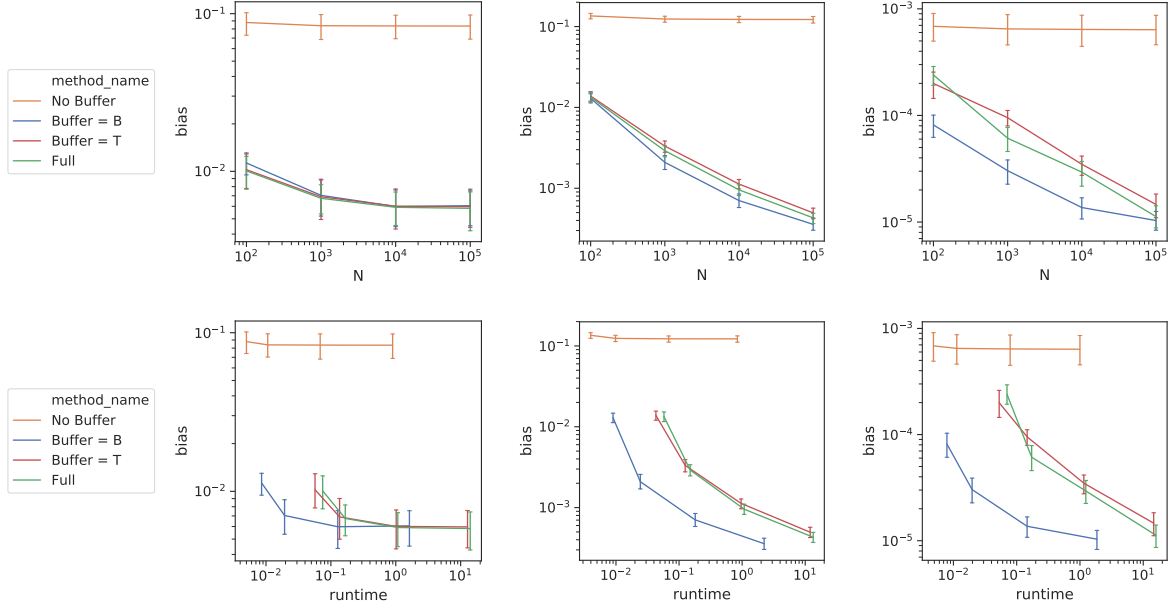


Figure 4: Stochastic gradient bias varying N for different S, B . (left) LGSSM ϕ , (middle) SVM ϕ , (right) GARCH β . (top) x -axis is N , (bottom) x -axis is runtime in seconds. **No Buffer** is $g^{\text{PF}}(16, 0, N)$, **Buffer $B = B$** is $g^{\text{PF}}(16, B, N)$, **Buffer $B = T$** is $g^{\text{PF}}(16, T, N)$, and **Full** is $g^{\text{PF}}(T, T, N)$. The moderate buffer size $B = 8$ for LGSSM and GARCH and $B = 16$ for the SVM. Error bars are 95% CI over 1000 replications.

In the Appendix, we present plots of the bias varying B, S, N using PaRIS instead of the naive PF. We find that PaRIS performs similarly to the naive PF for the small subsequence lengths $|\mathcal{S}^*|$ considered, while taking ≈ 10 times longer to run.

5.3 SGLD Experiments

Having examined the stochastic gradient bias, we now examine using our buffered stochastic gradient estimators in SGLD (Algorithm 2).

5.3.1 SGLD Evaluation Methods

We assess the performance of our samplers given a fixed computation budget, by measuring both the heldout and predictive loglikelihoods on a test sequence. Given a sampled parameter value θ the heldout loglikelihood is

$$\sum_{t=1}^T \log p(y_t | y_{<t}, \theta) \approx \sum_{t=1}^T \sum_{i=1}^N w_{t-1}^{(i)} \log p(y_t | x_{t-1}^{(i)}, \theta), \quad (28)$$

and the r -step ahead predictive loglikelihood is

$$\sum_{t=1}^T \log p(y_{t+r} | y_{<t}, \theta) \approx \sum_{t=1}^T \sum_{i=1}^N w_{t-1}^{(i)} \log p(y_{t+r} | x_{t-1}^{(i)}, \theta), \quad (29)$$

where $\{x_t^{(i)}, w_t^{(i)}\}_{i=1}^N$ are obtained from the particle filter on the test sequence. For synthetic data, we also measure the MSE of SGLD’s finite sample averages $\hat{\theta}_{(K)} = \sum_{k \leq K} \theta^{(k)}/K$ to the true parameters θ^* .

We measure the sample quality of our MCMC chains $\{\theta^{(k)}\}_{k=1}^K$ using the *kernel Stein discrepancy* (KSD) for equal compute time (Gorham and Mackey, 2017; Liu et al., 2016). We choose to use KSD rather than classic MCMC diagnostics such as effective sample size (ESS) (Gelman et al., 2013), because KSD penalizes the bias present in our MCMC chains. Given a sample chain (after burnin and thinning) $\{\theta^{(k)}\}_{k=1}^{\tilde{K}}$, let $\hat{p}(\theta|y)$ be the empirical distribution of the samples. Then the KSD between $\hat{p}(\theta|y)$ and the posterior distribution $p(\theta|y)$ is

$$\text{KSD}(\hat{p}, p) = \sum_{d=1}^{\dim(\theta)} \sqrt{\sum_{k, k'=1}^{\tilde{K}} \frac{\mathcal{K}_0^d(\theta^{(k)}, \theta^{(k')})}{\tilde{K}^2}}, \quad (30)$$

where

$$\mathcal{K}_0^d(\theta, \theta') = \frac{1}{p(\theta|y)p(\theta'|y)} \nabla_{\theta_d} \nabla_{\theta'_d} (p(\theta|y) \mathcal{K}(\theta, \theta') p(\theta'|y)) \quad (31)$$

and $\mathcal{K}(\cdot, \cdot)$ is a valid kernel function. Following Gorham and Mackey (2017), we use the inverse multiquadratic kernel $\mathcal{K}(\theta, \theta') = (1 + \|\theta - \theta'\|_2^2)^{-0.5}$ in our experiments. Since Eq. (31) requires full gradient evaluations

of $\log p(\theta|y)$ that are computationally intractable, we replace these terms with corresponding stochastic estimates using g_θ^{PF} .

5.3.2 SGLD on Synthetic LGSSM Data

To assess the effect of using particle filters with buffered stochastic gradients, we first focus on SGLD on synthetic LGSSM data, where calculating $\hat{g}_\theta(S, B)$ is possible. We generate training sequences of length $T = 10^3$ or 10^6 and test sequences of length $T = 10^3$ using the same parametrization as Section 5.2.

We consider three pairs of different gradient estimators: **Full** ($S = T$), **Buffered** ($S = 40, B = 10$) and **No Buffer** ($S = 40, B = 0$) each with $N = 1000$ particles using the particle filter and with $N = \infty$ using the Kalman filter. To select the stepsize, we performed a grid search over $\epsilon \in \{1, 0.1, 0.01, 0.001\}$ and selected the method with smallest KSD to the posterior on the training set. We present the KSD results (for the best ϵ) in Table 2 and trace plots of the metrics in Figure 5.

From Figure 5, we see that the methods without buffering ($B = 0$) have lower heldout loglikelihoods on the test sequence and have higher MSE as they are biased. We also see that the full sequence methods ($S = T$) perform poorly for large $T = 10^6$.

The KSD results further support this story. Table 2 presents the mean and standard deviation on our estimated \log_{10} KSD for θ . Tables of the marginal KSD for individual components of θ can be found in the Appendix. The methods without buffering have larger KSD, as the inherent bias of $\hat{g}_\theta(S, B = 0)$ led to an incorrect stationary distribution. The full sequence methods perform poorly for $T = 10^6$ because of a lack of samples that can be computed in a fixed runtime.

Table 2: KSD for Synthetic LGSSM. Mean and SD.

S	B	N	\log_{10} KSD	
			$T = 10^3$	$ T = 10^6$
T	-	1000	0.85 (0.08)	4.92 (0.40)
		∞	0.64 (0.17)	4.85 (0.36)
40	0	1000	1.58 (0.03)	4.68 (0.10)
		∞	1.55 (0.03)	4.68 (0.11)
40	10	1000	0.68 (0.25)	3.43 (0.19)
		∞	0.61 (0.21)	3.25 (0.29)

In the Appendix, we present similar results on synthetic SVM and GARCH data. Also in the Appendix, we present results on LGSSM in higher dimensions. As

is typical in the particle filtering literature, the performance degrades with increasing dimensions for N fixed.

5.3.3 SGLD on Exchange Rate Log-Returns

We now consider fitting the SVM and the GARCH model to EUR-USD exchange rate data at the minute resolution from November 2017 to October 2018. The data consists of 350,000 observations of demeaned log-returns. As the market is closed during non-business hours, we further break the data into 53 weekly segments of roughly 7,000 observations each. In our model, we assume independence between weekly segments and divide the data into a training set of the first 45 weeks and a test set of the last 8 weeks. Full processing details and example plots are in the Appendix. Note that our method (Algorithm 2) easily scales to the unsegmented series; however the abrupt changes between starts of weeks are not adequately modeled by Eq. (26)

We fit both the SVM and the GARCH model using SGLD with four different gradient methods: (i) **Full**, the full gradient over all segments in the training set; (ii) **Weekly**, a stochastic gradient over a randomly selected segment in the training set; (iii) **No Buffer**, a stochastic gradient over a randomly selected *subsequence* of length $S = 40$; and (iv) **Buffer**, our buffered stochastic gradient for a subsequence of length $S = 40$ with buffer length $B = 10$. To estimate the stochastic gradients, we use Algorithm 1 with $N = 1000$. To select the stepsize parameter, we performed a grid search over $\epsilon \in \{1, 0.1, 0.01, 0.001\}$ and selected the method with smallest KSD. We present the KSD results in Table 3. Figure 6 are trace plots of the heldout and predictive loglikelihood for the four different SGLD methods, each averaged over 5 chains.

Table 3: KSD for SGLD on exchange rate data. Mean and SD over 5 chains each.

METHOD	\log_{10} KSD	
	SVM	GARCH
FULL	4.03 (0.14)	2.84 (0.30)
WEEKLY	3.87 (0.08)	2.81 (0.21)
NO BUFFER	4.48 (0.01)	2.09 (0.09)
BUFFER	3.56 (0.08)	2.19 (0.05)

For the SVM, we see that buffering improves performance on both heldout and predictive loglikelihoods, Figure 6 (top), and also leads to more accurate MCMC samples, Table 3 (left). In particular, the samples from SGLD without buffering have smaller ϕ, τ^2 and a larger

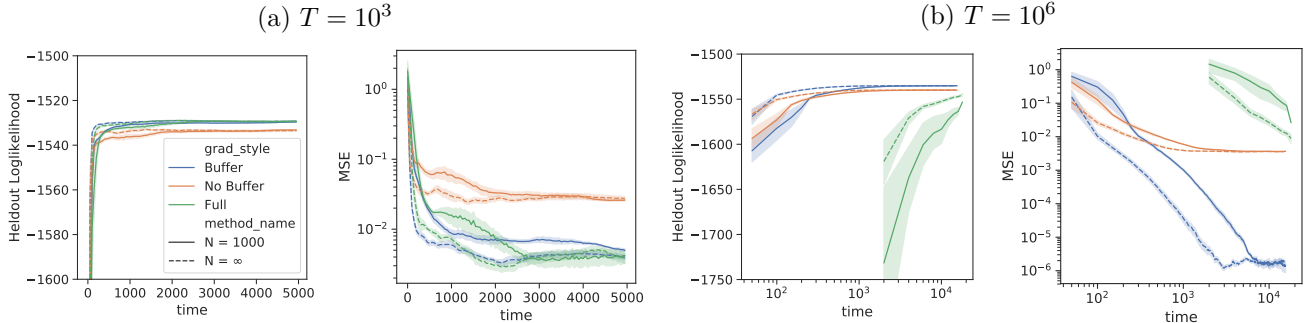


Figure 5: Comparison of SGLD with different gradient estimates on synthetic LGSSM data: $T = 10^3$ (left-pair), $T = 10^6$ (right-pair). (Left) heldout-loglikelihood, (Right) MSE of estimated posterior mean to true $\phi = 0.9$.

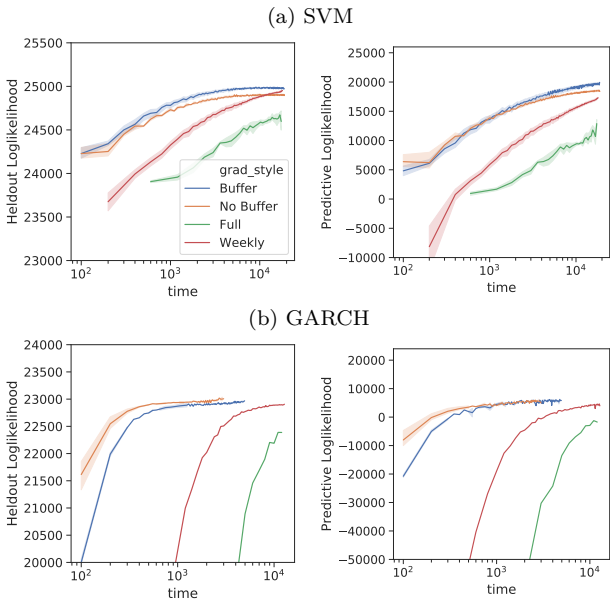


Figure 6: Comparison of SGLD with different gradient estimates on the exchange rate data: heldout-loglikelihood (left), 3-step ahead predictive loglikelihood (right).

σ^2 , indicating that its posterior is (inaccurately) centered around a SVM with larger latent state noise. We also again see that the full sequence and weekly segment methods perform poorly due to the limited number of samples that can be computed in a fixed runtime.

For the GARCH model, Figure 6 (bottom) and Table 3 (right), we see that the subsequence methods outperform the full sequence methods, but unlike in the SVM, buffering does not help with inference on the GARCH data. This is because the GARCH model that we recover on the exchange rate data (for all gradient methods) is close to white noise $\beta \approx 0$. Therefore the

model believes the observations are close to independent, hence no buffer is necessary. Although buffering performs worse on a runtime scale, here, it is leading to a more accurate posterior estimate (less bias) in *all* settings.

6 Discussion

In this work, we developed a particle buffered stochastic gradient estimators for nonlinear SSMs. Our key contributions are (i) extending buffered stochastic gradient MCMC with particle filtering for nonlinear SSMs, (ii) analyzing the error of our proposed particle buffered stochastic gradient g_θ^{PF} (Theorem 2) and its affect on our SGLD Algorithm 2 (Theorem 1), and (iii) generalizing the geometric decay bound for buffering to nonlinear SSMs with log-concave likelihoods (Theorem 3). We evaluated our proposed gradient estimator with SGLD on both synthetic data and EUR-USD exchange rate data. We find that buffering is necessary to control bias and that our stochastic gradient methods (Algorithm 2) are able to out perform batch methods on long sequences.

Possible future extensions of this work include relaxing the log-concave restriction of Theorem 3, extensions to Algorithm 2 as discussed at the end of Section 3.2, and applying our particle buffered stochastic gradient estimates to other applications than SGMCMC, such as optimization in variational autoencoders for sequential data (Maddison et al., 2017; Naesseth et al., 2018).

Acknowledgements

We would like to thank Nicholas Foti for helpful discussions. This work was supported in part by ONR Grants N00014-15-1-2380 and N00014-18-1-2862, NSF CAREER Award IIS-1350133, and EPSRC

Grants EP/L015692/1, EP/S00159X/1, EP/R01860X/1, EP/R018561/1 and EP/R034710/1.

References

Christopher Aicher, Yi-An Ma, Nicholas J. Foti, and Emily B. Fox. Stochastic Gradient MCMC for State Space Models. *arXiv preprint arXiv:1810.09098*, 2018.

Christophe Andrieu, Arnaud Doucet, and Roman Holenstein. Particle Markov chain Monte Carlo methods. *Journal of the Royal Statistical Society: Series B (Statistical Methodology)*, 72(3):269–342, 2010.

Jack Baker, Paul Fearnhead, Emily B Fox, and Christopher Nemeth. Control variates for stochastic gradient MCMC. *Statistics and Computing*, Aug 2018. ISSN 1573-1375.

Tim Bollerslev. Generalized autoregressive conditional heteroskedasticity. *Journal of Econometrics*, 31(3): 307 – 327, 1986. ISSN 0304-4076.

Olivier Cappé, Eric Moulines, and Tobias Rydén. *Inference in Hidden Markov Models*. Springer, 2005.

Niladri S Chatterji, Nicolas Flammarion, Yi-An Ma, Peter L Bartlett, and Michael I Jordan. On the Theory of Variance Reduction for Stochastic Gradient Monte Carlo. In *Proceedings of the 35th International Conference on Machine Learning*, pages 764–773, 2018.

Changyou Chen, Nan Ding, and Lawrence Carin. On the convergence of stochastic gradient MCMC algorithms with high-order integrators. In *Advances in Neural Information Processing Systems*, pages 2278–2286, 2015.

Tianqi Chen, Emily Fox, and Carlos Guestrin. Stochastic gradient Hamiltonian Monte Carlo. In *International Conference on Machine Learning*, pages 1683–1691, 2014.

Maria Colombo, Alessio Figalli, and Yash Jhaveri. Lipschitz changes of variables between perturbations of log-concave measures. *arXiv preprint arXiv:1510.03687*, 2015.

Johan Dahlin, Fredrik Lindsten, and Thomas B Schön. Particle Metropolis–Hastings using gradient and Hessian information. *Statistics and Computing*, 25(1): 81–92, 2015.

Arnak S Dalalyan and Avetik G Karagulyan. User-friendly guarantees for the Langevin Monte Carlo with inaccurate gradient. *arXiv preprint arXiv:1710.00095*, 2017.

Nan Ding, Youhan Fang, Ryan Babbush, Changyou Chen, Robert D Skeel, and Hartmut Neven. Bayesian sampling using stochastic gradient thermostats. In *Advances in Neural Information Processing Systems*, pages 3203–3211, 2014.

Arnaud Doucet and Adam M Johansen. A tutorial on particle filtering and smoothing: Fifteen years later. *Handbook of Nonlinear Filtering*, 12(656-704):3, 2009.

Vanja Dukic, Hedibert F Lopes, and Nicholas G Polson. Tracking epidemics with Google flu trends data and a state-space SEIR model. *Journal of the American Statistical Association*, 107(500):1410–1426, 2012.

Paul Fearnhead and Hans R. Künsch. Particle Filters and Data Assimilation. *Annual Review of Statistics and Its Application*, 5(1):421–449, 2018.

Andrew Gelman, John B Carlin, Donald B Rubin, Aki Vehtari, David B Dunson, and Hal S Stern. *Bayesian Data Analysis*. CRC Press, 2013.

Mark Girolami and Ben Calderhead. Riemann manifold Langevin and Hamiltonian Monte Carlo methods. *Journal of the Royal Statistical Society: Series B (Statistical Methodology)*, 73(2):123–214, 2011.

N. J. Gordon, D. J. Salmond, and A. F. M. Smith. Novel approach to nonlinear/non-Gaussian Bayesian state estimation. *IEE Proceedings F - Radar and Signal Processing*, 140(2):107–113, 1993.

Jackson Gorham and Lester Mackey. Measuring Sample Quality with Kernels. *arXiv preprint arXiv:1703.01717*, 2017.

Nikolas Kantas, Arnaud Doucet, Sumeetpal S Singh, Jan Maciejowski, Nicolas Chopin, et al. On particle methods for parameter estimation in state-space models. *Statistical science*, 30(3):328–351, 2015.

Gregor Kastner. Dealing with stochastic volatility in time series using the R package stochvol. *Journal of Statistical Software*, 69(5):1–30, 2016. doi: 10.18637/jss.v069.i05.

Genshiro Kitagawa. Monte Carlo filter and smoother for non-Gaussian nonlinear state space models. *Journal of Computational and Graphical Statistics*, 5(1):1–25, 1996.

Genshiro Kitagawa and Seisho Sato. Monte Carlo smoothing and self-organising state-space model. In *Sequential Monte Carlo Methods in Practice*, pages 177–195. Springer, 2001.

Roland Langrock. Some applications of nonlinear and non-Gaussian state-space modelling by means of hidden Markov models. *Journal of Applied Statistics*, 38(12):2955–2970, 2011.

Jun S. Liu and Rong Chen. Sequential Monte Carlo methods for Dynamic Systems. *Journal of the American Statistical Association*, 93(443):1032–1044, 1998.

Qiang Liu, Jason Lee, and Michael Jordan. A kernelized Stein discrepancy for goodness-of-fit tests. In *International Conference on Machine Learning*, pages 276–284, 2016.

Yi-An Ma, Tianqi Chen, and Emily Fox. A complete recipe for stochastic gradient MCMC. In *Advances in Neural Information Processing Systems*, pages 2917–2925, 2015.

Yi-An Ma, Nicholas J Foti, and Emily B Fox. Stochastic Gradient MCMC Methods for Hidden Markov Models. In *International Conference on Machine Learning*, pages 2265–2274, 2017.

Chris J Maddison, John Lawson, George Tucker, Nicolas Heess, Mohammad Norouzi, Andriy Mnih, Arnaud Doucet, and Yee Teh. Filtering variational objectives. In *Advances in Neural Information Processing Systems*, pages 6573–6583, 2017.

Christian Naesseth, Scott Linderman, Rajesh Ranganath, and David Blei. Variational Sequential Monte Carlo. In *International Conference on Artificial Intelligence and Statistics*, pages 968–977, 2018.

Tigran Nagapetyan, Andrew B Duncan, Leonard Hasenclever, Sebastian J Vollmer, Lukasz Szpruch, and Konstantinos Zygalakis. The true cost of stochastic gradient Langevin dynamics. *arXiv preprint arXiv:1706.02692*, 2017.

Christopher Nemeth and Paul Fearnhead. Stochastic gradient markov chain monte carlo. *arXiv preprint arXiv:1907.06986*, 2019.

Christopher Nemeth, Paul Fearnhead, and Lyudmila Mihaylova. Particle approximations of the score and observed information matrix for parameter estimation in state-space models with linear computational cost. *Journal of Computational and Graphical Statistics*, 25(4):1138–1157, 2016.

Jimmy Olsson and Johan Westerborn. Efficient particle-based online smoothing in general hidden Markov models: the PaRIS algorithm. *Bernoulli*, 23(3):1951–1996, 2017.

Rihui Ou, Alexander L Young, and David B Dunson. Clustering-Enhanced Stochastic Gradient MCMC for Hidden Markov Models with Rare States. *arXiv preprint arXiv:1810.13431*, 2018.

Sam Patterson and Yee Whye Teh. Stochastic gradient Riemannian Langevin dynamics on the probability simplex. In *Advances in Neural Information Processing Systems*, pages 3102–3110, 2013.

George Poyiadjis, Arnaud Doucet, and Sumeetpal S Singh. Particle approximations of the score and observed information matrix in state space models with application to parameter estimation. *Biometrika*, 98(1):65–80, 2011.

Herbert Robbins and Sutton Monro. A stochastic approximation method. *The Annals of Mathematical Statistics*, pages 400–407, 1951.

Adrien Saumard and Jon A Wellner. Log-concavity and strong log-concavity: a review. *Statistics surveys*, 8:45, 2014.

Mark Schmidt, Reza Babanezhad, Mohamed Ahmed, Aaron Defazio, Ann Clifton, and Anoop Sarkar. Non-uniform stochastic average gradient method for training conditional random fields. In *Artificial Intelligence and Statistics*, pages 819–828, 2015.

Neil Shephard. *Stochastic Volatility: Selected Readings*. Oxford University Press, 2005.

Yee Whye Teh, Alexandre H Thiery, and Sebastian J Vollmer. Consistency and fluctuations for stochastic gradient Langevin dynamics. *The Journal of Machine Learning Research*, 17(1):193–225, 2016.

Cédric Villani. *Optimal transport: old and new*, volume 338. Springer Science & Business Media, 2008.

Sebastian J Vollmer, Konstantinos C Zygalakis, and Yee Whye Teh. Exploration of the (non-) asymptotic bias and variance of stochastic gradient Langevin dynamics. *The Journal of Machine Learning Research*, 17(1):5504–5548, 2016.

Max Welling and Yee W Teh. Bayesian learning via stochastic gradient Langevin dynamics. In *Proceedings of the 28th International Conference on Machine Learning (ICML-11)*, pages 681–688, 2011.

Appendix

This Appendix is organized as follows. In Section A, we provide additional details and proofs for the error analysis of Section 4. In particular, we provide the proof of Theorem 1 in Section A.1, the proof of Theorem 2 in Section A.2, the proof of Theorem 3 in Section A.3 and applications of Theorem 3 for LGSSM and SVM in Section A.4. In Section B, we provide additional particle filter and gradient details for the models in Section 5.1. In Section C, we provide additional details and figures of experiments.

A Error Analysis Proofs

A.1 Proof of Theorem 1

We now prove the error bounds for biased SGLD's finite sample average found in Section 4.1. The proof is a modification of the proof of Theorem 3 found in Appendix E of Chen et al. (2015).

We first review the condition the test statistic ϕ must satisfy. Let \mathcal{L} be the generator of the Langevin diffusion

$$\mathcal{L}[\psi(\theta_t)] = \nabla U(\theta_t) \cdot \nabla \psi(\theta_t) + \frac{\epsilon^2}{2} \text{tr}(\nabla^2 \psi(\theta_t)) .$$

Then, we define ψ to solve the *Poisson equation*

$$\frac{1}{K} \sum_{k=1}^K \mathcal{L}[\psi(\theta^{(k)})] = \hat{\phi}_{K,\epsilon} - \bar{\phi} , \quad (\text{A.1})$$

where we recall

$$\hat{\phi}_{K,\epsilon} = K^{-1} \sum_{k=1}^K \phi(\theta^{(k)}) \quad \text{and} \quad \bar{\phi} = \mathbb{E}_{p(\theta|y)}[\phi(\theta)] .$$

Our assumption on ϕ is that $\psi(\theta)$ and its derivatives are bounded by some finite constant M . This is the implicit moment condition for ϕ , which is also assumed by Vollmer et al. (2016) and Chen et al. (2015).

The proof of Theorem 1 then proceeds as in Theorem 3 of (Chen et al., 2015), except that we allow for a $\delta > 0$ such that $\mathbb{E} \|\hat{g}(\theta) - g(\theta)\| \leq \delta$ for all θ rather than restrict $\delta = 0$.

For compactness of notation, we will use g_k to denote $g(\theta^{(k)})$, \hat{g}_k to denote $\hat{g}(\theta^{(k)})$, and ψ_k to denote $\psi(\theta^{(k)})$.

Proof of Theorem 1. Following (Chen et al., 2015), from the definition of the functional ψ and generator \mathcal{L} , we have

$$\begin{aligned} \hat{\phi}_{K,\epsilon} - \bar{\phi} &= \frac{\mathbb{E} \psi_K - \psi_1}{K\epsilon} - \frac{\sum_{k=1}^K (\mathbb{E} \psi_k - \psi_k)}{K\epsilon} \\ &\quad + \frac{\sum_{k=1}^K (\hat{g}_k - g_k) \cdot \nabla \psi_k}{K} + \mathcal{O}(\epsilon) , \quad (\text{A.2}) \end{aligned}$$

and we also have $\mathbb{E} \psi_K - \mathbb{E} \psi_1$ is $\mathcal{O}(1)$, $\mathbb{E} (\mathbb{E} \psi_K - \psi_1)^2$ is $\mathcal{O}(1)$, and $\mathbb{E} (\mathbb{E} \psi_k - \psi_k)^2$ is $\mathcal{O}(\epsilon)$.

Let $\xi_k = (\hat{g}_k - g_k) \cdot \nabla \psi_k$. From our assumptions on the bias and MSE of \hat{g} and as $\nabla \psi$ is bounded, we have $|\mathbb{E} \xi_k| \leq M\delta$ and $\mathbb{E} [\xi_k^2] \leq M^2\sigma^2$ for all k . In addition, we have for all $k \neq k'$

$$|\mathbb{E} [\xi_k \xi_{k'}]| \leq M^2 \|\mathbb{E} [\hat{g}_k - g_k]\| \|\mathbb{E} [\hat{g}_{k'} - g_{k'}]\| \leq M^2 \delta^2 , \quad (\text{A.3})$$

where the expectations are over *independent* stochastic subsequences \mathcal{S} chosen at steps k and k' .

To prove the bias bound, we take the expectation of Eq. (A.2) and bound each term

$$|\mathbb{E} \hat{\phi}_{K,\epsilon} - \bar{\phi}| = \mathcal{O} \left(\frac{1}{K\epsilon} + \delta + \epsilon \right) \quad (\text{A.4})$$

To prove the MSE bound, we take the square and expectation of both sides of Eq. (A.2),

$$\begin{aligned} \mathbb{E} (\hat{\phi}_{K,\epsilon} - \bar{\phi})^2 &\leq \\ &\mathbb{E} \left[\frac{(\mathbb{E} \psi_K - \psi_0))^2}{K^2 \epsilon^2} + \frac{\sum_{k=1}^K (\mathbb{E} \phi_k - \psi_k)^2}{K^2 \epsilon^2} \right. \\ &+ \frac{\sum_{k=1}^K \xi_k^2 + \sum_{k \neq k'=1}^K \xi_k \xi_{k'}}{K^2} + \mathcal{O}(\epsilon^2) \\ &+ \frac{\sum_{k=1}^K \xi_k}{K} \cdot \left(\frac{\mathbb{E} \psi_K - \psi_1}{K\epsilon} \right. \\ &\quad \left. \left. - \frac{\sum_{k=1}^K (\mathbb{E} \psi_k - \psi_k)}{K\epsilon} + \mathcal{O}(\epsilon) \right) \right] \quad (\text{A.5}) \end{aligned}$$

The first two lines are the squared terms and the last two lines are the cross terms that do not go to zero. In particular, we do not assume $\hat{g}(\theta)$ is unbiased for $g(\theta)$, therefore we keep the cross-terms involving ξ_k . Bounding each term of Eq. (A.5) gives the MSE bound

$$\begin{aligned} \mathbb{E} (\hat{\phi}_{K,\epsilon} - \bar{\phi})^2 &\leq \frac{\mathcal{O}(1)}{K^2 \epsilon^2} + \frac{\mathcal{O}(K\epsilon)}{K^2 \epsilon^2} + \frac{\mathcal{O}(K\sigma^2) + \mathcal{O}(K^2\delta^2)}{K^2} + \mathcal{O}(\epsilon^2) \\ &\quad + \mathcal{O}(\delta) \cdot \left(\frac{\mathcal{O}(1)}{K\epsilon} + \frac{\mathcal{O}(K)}{K\epsilon} + \mathcal{O}(\epsilon) \right) \\ &\leq \mathcal{O} \left(\frac{1}{K\epsilon} + \frac{\sigma^2}{K} + \epsilon^2 + \delta^2 + \frac{\delta}{\epsilon} + \delta\epsilon \right) . \quad (\text{A.6}) \end{aligned}$$

□

A.2 Proof of Theorem 2

We now prove Theorem 2, which bounds the bias and MSE of our buffered stochastic gradient $g_\theta^{\text{PF}}(S, B, N)$. In

our proof, we use Lemma A.1 to bound the subsequence error which is proved in Section A.2.1.

Proof of Theorem 2. For the bias bound, (17), we apply the triangle inequality to decompose the error into three terms

$$\begin{aligned} \|\mathbb{E} g_\theta^{\text{PF}}(S, B, N) - g_\theta\| &\leq \\ &\underbrace{\|\mathbb{E} (g_\theta^{\text{PF}}(S, B, N) - \hat{g}_\theta(S, B))\|}_{\text{particle bias (I)}} \\ &+ \underbrace{\|\mathbb{E} (\hat{g}_\theta(S, B) - \hat{g}_\theta(S, T))\|}_{\text{buffering bias (II)}} \\ &+ \underbrace{\|\mathbb{E} \hat{g}_\theta(S, T) - g_\theta\|}_{\text{subsequence bias (III)}}, \end{aligned} \quad (\text{A.7})$$

where expectations are over the random subsequence \mathcal{S} and particles. Each term is bounded separately (recalling that $\gamma = \max_t \Pr(t \in \mathcal{S})^{-1}$)

- (I) *Particle bias:* the particle filter bias is $\mathcal{O}(\gamma \frac{S+2B}{N})$ (see Eq. 3.15 of (Kantas et al., 2015)).
- (II) *Buffering bias:* from (Aicher et al., 2018), we know there exists a finite constant $C_1 < \infty$ that is independent of T, S, B, N , such that

$$\mathbb{E} \|\hat{g}(S, B) - \hat{g}(S, T)\| \leq \gamma \cdot C_1 \cdot (L_\theta)^B. \quad (\text{A.8})$$

Thus, the buffering bias can be upper bounded using Jensen's inequality

$$\begin{aligned} \|\mathbb{E} (\hat{g}(S, B) - \hat{g}(S, T))\| &\leq \mathbb{E} \|\hat{g}(S, B) - \hat{g}(S, T)\| \\ &\leq \gamma \cdot C_1 \cdot (L_\theta)^B. \end{aligned} \quad (\text{A.9})$$

- (III) *Subsequence bias:* the subsequence bias is zero as $\mathbb{E} \hat{g}_\theta(S, T) = g_\theta$.

Applying these bounds gives us the bias bound

$$\|\mathbb{E} g_\theta^{\text{PF}}(S, B, N) - g_\theta\| \leq \gamma \cdot \left[C_1 (L_\theta)^B + \mathcal{O}\left(\frac{S+2B}{N}\right) \right]. \quad (\text{A.10})$$

For the MSE bound, (18), we again apply the triangle inequality and recall that $2XY \leq X^2 + Y^2$ implies $(X + Y + Z)^2 \leq 3(X^2 + Y^2 + Z^2)$ to decompose the error into three terms

$$\begin{aligned} \mathbb{E} \|g_\theta^{\text{PF}}(S, B, N) - g_\theta\|^2 &\leq \\ &3 \underbrace{\mathbb{E} \|g_\theta^{\text{PF}}(S, B, N) - \hat{g}_\theta(S, B)\|^2}_{\text{particle MSE (I)}} \\ &+ 3 \underbrace{\mathbb{E} \|\hat{g}_\theta(S, B) - \hat{g}_\theta(S, T)\|^2}_{\text{buffering MSE (II)}} \\ &+ 3 \underbrace{\mathbb{E} \|\hat{g}_\theta(S, T) - g_\theta\|^2}_{\text{subsequence MSE (III)}}, \end{aligned} \quad (\text{A.11})$$

where expectations are over the random subsequence \mathcal{S} and particles. Again, each term is bounded separately,

- (I) *Particle MSE:* the particle filter MSE bound is $\mathcal{O}(\gamma^2 \frac{(S+2B)^2}{N})$ (see Eq. 3.15 of (Kantas et al., 2015)).
- (II) *Buffering MSE:* from (Aicher et al., 2018), the buffering MSE is bounded

$$\mathbb{E} \|\hat{g}_\theta(S, B) - \hat{g}_\theta(S, T)\|^2 \leq \gamma^2 \cdot C_1^2 \cdot (L_\theta)^{2B}. \quad (\text{A.12})$$

- (III) *Subsequence MSE:* from Lemma A.1, there exists a constant $C_2 < \infty$ independent of T, S, B, N such that

$$\mathbb{E} \|\hat{g}_\theta(S, T) - g_\theta\|^2 \leq \gamma^2 \cdot C_2 \cdot S. \quad (\text{A.13})$$

Combining these bounds gives us the MSE bound

$$\begin{aligned} \mathbb{E} \|g_\theta^{\text{PF}}(S, B, N) - g_\theta\|^2 &\leq \\ &3\gamma^2 \cdot \left[C_1^2 (L_\theta)^{2B} + C_2 S + \mathcal{O}\left(\frac{(S+2B)^2}{N}\right) \right]. \end{aligned} \quad (\text{A.14})$$

□

A.2.1 Stochastic Subsequence MSE

For the proof of Theorem 2, we bound the MSE between the full gradient g_θ and the unbiased stochastic gradient estimate $\hat{g}_\theta(S, T)$, specifically for the case of randomly sampling a *contiguous* subsequence \mathcal{S} . Because $\hat{g}_\theta(S, T)$ is unbiased for g_θ , this reduces to calculating the variance of $\hat{g}_\theta(S, T)$ with respect to the sampling distribution of the subsequence \mathcal{S} .

Let f_t denote the t -th gradient term in Fisher's identity

$$f_t = \mathbb{E}_{x_{1:T} | y_{1:T}, \theta} [\nabla \log p(y_t, x_t | x_{t-1}, \theta)] \quad (\text{A.15})$$

Therefore

$$g_\theta = \sum_{t=1}^T f_t \quad \text{and} \quad \hat{g}_\theta(S, T) = \sum_{t \in \mathcal{S}} \Pr(t \in \mathcal{S})^{-1} \cdot f_t$$

We now present the lemma that bounds the variance of $\hat{g}_\theta(S, T)$, under the assumption that the autocorrelation of f_t decays geometrically $|\text{Corr}(f_t, f_{t+s})| \leq \rho^s$.

Lemma A.1. *If for all t , the variance of f_t is bounded and the autocorrelation of f_t is geometrically bounded, then there exists a constant $C_2 < \infty$ (not dependent on T, S, B, N) such that*

$$\text{Var}(\hat{g}_\theta(S, T)) \leq \gamma^2 \cdot C_2 \cdot S. \quad (\text{A.16})$$

The assumption that the autocorrelation of f_t decays geometrically is reasonable when both the observations $Y_{1:T}$ and the posterior latent states $X_{1:T}|Y_{1:T}$ are *ergodic* (i.e. exhibit an exponential forgetting property) (Cappé et al., 2005).

We now present the proof.

Proof of Lemma A.1. Let $V < \infty$ be a bound on the variance of f_t for all t (i.e. $\text{Var}(f_t) \leq V$). Let $\rho \in [0, 1)$ be a bound on the geometric decay of the autocorrelation of f_t . Then we have $|\text{Corr}(f_t, f_{t+s})| \leq \rho^s$ for all t and $s \in \mathbb{N}$. Together these bounds imply a bound on the covariance between any f_t and f_{t+s}

$$\begin{aligned} \text{CoV}(f_t, f_{t+s}) &\leq |\text{Corr}(f_t, f_{t+s})| \cdot \sqrt{\text{Var}(f_t) \cdot \text{Var}(f_{t+s})} \\ &\leq V \rho^s. \end{aligned} \quad (\text{A.17})$$

Then we have

$$\begin{aligned} \text{Var}(\hat{g}_\theta(S, T)) &\leq \gamma^2 \cdot \text{Var} \left[\sum_{t \in \mathcal{S}} f_t \right] \\ &= \gamma^2 \cdot \left[\sum_{t \in \mathcal{S}} \text{Var}(f_t) + \sum_{t \neq t' \in \mathcal{S}} \text{CoV}(f_t, f_{t'}) \right], \\ &\leq \gamma^2 \cdot \left[S \cdot V + \sum_{s=1}^{S-1} 2(S-s) \cdot V \rho^s \right] \\ &= \gamma^2 \cdot S \cdot \left[V + 2V \sum_{s=1}^{S-1} (1-s/S) \cdot \rho^s \right] \\ &\leq \gamma^2 \cdot S \cdot \left[2V \sum_{s=0}^{S-1} \rho^s \right] \\ &\leq \gamma^2 \cdot S \cdot 2V/(1-\rho) \end{aligned} \quad (\text{A.18})$$

$$(\text{A.19})$$

As $S \geq 1$, if $C_2 = 2V/(1-\rho)$, we have

$$\mathbb{E} \|\hat{g}_\theta(S, T) - g_\theta\|^2 = \text{Var}(\hat{g}_\theta(S, T)) \leq \gamma^2 \cdot S \cdot C_2. \quad (\text{A.20})$$

□

A.3 Proof of Theorem 3

Theorem 3 states that if the prior distribution for x_0 , the transition distribution $p(x_t | x_{t-1}, \theta)$ and the emission distribution $p(y_t | x_t)$ are log-concave, then we can bound the Lipschitz constant of $\tilde{\Psi}_t$ in terms of $\tilde{\Psi}_t^{(0)}$ and $\tilde{\Psi}_t^{(1)}$.

We first briefly review Wasserstein distance, random mappings, and Lipschitz constants of kernels (Villani, 2008; Aicher et al., 2018). Then we review *Caffarelli's log-concave perturbation theorem*, the main tool we use in our proof. Finally, we present the proof in Section A.3.3.

A.3.1 Wasserstein Distance and Random Maps

The p -Wasserstein distance with respect to Euclidean distance is

$$\mathcal{W}_p(\gamma, \tilde{\gamma}) := \left[\inf_{\xi} \int \|x - \tilde{x}\|_2^p d\xi(x, \tilde{x}) \right]^{1/p} \quad (\text{A.21})$$

where ξ is a joint measure or *coupling* over (x, \tilde{x}) with marginals $\int_x d\xi(x, \tilde{x}) = d\gamma(x)$ and $\int_{\tilde{x}} d\xi(x, \tilde{x}) = d\tilde{\gamma}(\tilde{x})$.

To bound the Wasserstein distance, we first must introduce the concept of a *random mapping* associated with a transition kernel.

Let $\Psi : \mathcal{U} \rightarrow \mathcal{V}$ be a transition kernel for random variables u and v , then for any measure $\mu(u)$ over \mathcal{U} , we define the induced measure $(\mu\Psi)(v)$ over \mathcal{V} as $(\mu\Psi)(v) = \int \Psi(u, v) \mu(du)$.

A *random mapping* ψ is a random function that maps \mathcal{U} to \mathcal{V} such that if $u \sim \mu$ then $\psi(u) \sim \mu\Psi$. For example, if $\Psi(u, v) = \mathcal{N}(v | u, 1)$, then a random mapping for Ψ is the identity function plus Gaussian noise $\psi(u) = u + \epsilon$, where $\epsilon \sim \mathcal{N}(0, 1)$. Note that if ψ is deterministic $(\mu\Psi)(v)$ is the *push-forward* measure of μ through the mapping ψ ; otherwise it is the average (or marginal) over ψ of push-forward measures (Villani, 2008).

We say the kernel has Lipschitz constant L with respect to Euclidean distance if

$$\|\Psi\|_{Lip} = L \Leftrightarrow \sup_{u, u'} \left\{ \frac{\mathbb{E}_\psi [\|\psi(u) - \psi(u')\|_2]}{\|u - u'\|_2} \right\} \leq L \quad (\text{A.22})$$

Note that L is an upper-bound on the *expected value* of Lipschitz constants for random instances of ψ .

These definitions are useful for proving bounds in Wasserstein distance. For example, we can show the kernel Ψ induces a contraction in p -Wasserstein distance if $\|\Psi\|_{Lip} < 1$. That is $\mathcal{W}_p(\mu\Psi, \tilde{\mu}\Psi) \leq \|\Psi\|_{Lip} \cdot \mathcal{W}_p(\mu, \tilde{\mu})$

$$\begin{aligned} \mathcal{W}_p(\mu\Psi, \tilde{\mu}\Psi)^p &= \inf_{\xi(\mu\Psi, \tilde{\mu}\Psi)} \int \|v - \tilde{v}\|_2^p d\xi(v, \tilde{v}) \\ &\leq \inf_{\xi(\mu, \tilde{\mu})} \int \|\psi(u) - \psi(\tilde{u})\|_2^p d\xi(u, \tilde{u}) df_K \\ &\leq \inf_{\xi(\mu, \tilde{\mu})} \int \|\Psi\|_{Lip}^p \cdot \|u - \tilde{u}\|_2^p d\xi(u, \tilde{u}) \\ &= \|\Psi\|_{Lip}^p \cdot \mathcal{W}_p(\mu, \tilde{\mu})^p. \end{aligned} \quad (\text{A.23})$$

A.3.2 Caffarelli's Perturbation Theorem

Caffarelli's log-concave perturbation theorem allows us to connect Lipschitz constants between kernels that are log-concave perturbations of one another.

Theorem A.1 (Caffarelli's). *Suppose $\gamma(x)$ is a log-concave measure for x and $\ell(x)$ is a log-concave function*

such that $\gamma'(x) = \ell(x)\gamma(x)$ is a probability measure over x . Then there exists a 1-Lipschitz mapping $T : \mathcal{X} \rightarrow \mathcal{X}$ such that if $x \sim \gamma(x)$ then $T(x) \sim \gamma'(x)$.

We can think of $\gamma(x)$ as a prior distribution $p(x)$, $\ell(x)$ as a normalized conditional likelihood $p(y|x)/p(y)$ and $\gamma'(x)$ as the posterior $p(x|y)$. As $\ell(x)$ is log-concave, we call $\gamma'(x)$ a *log-concave perturbation* of γ .

The original version of Caffarelli's log-concave perturbation theorem (Colombo et al., 2015; Saumard and Wellner, 2014) requires the prior $\gamma(x)$ to be *strongly* log-concave (e.g. a Gaussian) to show that the mapping T is a *strict* contraction $\|T\|_{Lip} < 1$; however this weaker version, Theorem A.1 in (Villani, 2008), is sufficient for our purposes.

A.3.3 Proof of Theorem 3

Using Theorem A.1, we can now prove Theorem 3.

Proof of Theorem 3. Let $\vec{\psi}_t, \vec{\psi}_t^{(0)}, \vec{\psi}_t^{(1)}$ be random mappings associated respectively with forward kernels $\vec{\Psi}_t, \vec{\Psi}_t^{(0)}, \vec{\Psi}_t^{(1)}$. Because the transition and emission distributions are log-concave and log-concavity is preserved under product and marginalization (Saumard and Wellner, 2014), $\vec{\Psi}_t, \vec{\Psi}_t^{(0)}, \vec{\Psi}_t^{(1)}$ are log-concave and $p(y_{t \geq} | x_t)$ and $p(y_{>t} | x_t)$ are also log-concave.

Since $p(y_{\geq t} | x_t)$ is log-concave, we can write $\vec{\Psi}_t$ as a log-concave perturbation of $\vec{\Psi}_t^{(0)}$,

$$\begin{aligned} \vec{\Psi}_t &= p(x_t | x_{t-1}, y_{t:T}, \theta) \propto p(y_{\geq t} | x_t) p(x_t | x_{t-1}, \theta) \\ &= p(y_{\geq t} | x_t) \cdot \vec{\Psi}_t^{(0)}. \end{aligned} \quad (\text{A.24})$$

Therefore, there exists $T_t^{(0)}$ with $\|T_t^{(0)}\|_{Lip} \leq 1$ such that $\vec{\psi}_t = (T_t^{(0)} \circ \vec{\psi}_t^{(0)})$. Thus,

$$\|\vec{\Psi}_t\|_{Lip} = \|T_t^{(0)}\|_{Lip} \cdot \|\vec{\Psi}_t^{(0)}\|_{Lip} \leq \|\vec{\Psi}_t^{(0)}\|_{Lip}. \quad (\text{A.25})$$

Similarly, we can write $\vec{\Psi}_t$ as a log-concave perturbation of $\vec{\Psi}_t^{(1)}$ using $p(y_{>t} | x_t)$, thus $\|\vec{\Psi}_t\|_{Lip} \leq \|\vec{\Psi}_t^{(1)}\|_{Lip}$.

$$\begin{aligned} \vec{\Psi}_t &= p(x_t | x_{t-1}, y_{t:T}, \theta) \propto p(y_{>t} | x_t) p(x_t | y_t, x_{t-1}, \theta) \\ &= p(y_{>t} | x_t) \cdot \vec{\Psi}_t^{(1)}. \end{aligned} \quad (\text{A.26})$$

□

Note the assumptions for equivalent results in the backward smoothers $\vec{\Psi}_t$ are identical. Log-concavity in $p(x_t | x_{t+1}, \theta)$ is implied from both $p(x_t | x_{t-1}, \theta)$ and the prior $p(x_t)$ being log-concave.

A.4 Bounds for Specific Models

We now provide specific bounds for the buffering error for models we consider in Section 5 (LGSSM and SVM) using Theorem 3.

For both the LGSSM and SVM, we assume the prior $\nu(x_0 | \theta) = \mathcal{N}(0, \sigma^2 / (1 - \phi^2))$. Then the latent state transitions are

$$\begin{aligned} p(x_t | x_{t-1}, \theta) &= \mathcal{N}(x_t | \phi x_{t-1}, \sigma^2) \\ p(x_t | x_{t+1}, \theta) &= \mathcal{N}(x_t | \phi x_{t+1}, \sigma^2), \end{aligned}$$

which are both Gaussian and therefore log-concave in x .

Similarly, the emissions for the LGSSM and SVM are also log-concave in x :

For the LGSSM,

$$p(y_t | x_t, \theta) \propto \exp\left(-\frac{(y_t - x_t)^2}{2\sigma^2}\right),$$

which is log-concave.

For the SVM,

$$p(y_t | x_t, \theta) \propto \exp\left(-\frac{y_t^2}{2\sigma^2} \cdot e^{-x_t} - \frac{x_t}{2}\right),$$

which is log-concave as e^{-x} is convex.

A.4.1 Contraction Bound for LGSSM

We assume the prior $\nu(x_0 | \theta) = \mathcal{N}(0, \sigma^2 / (1 - \phi^2))$. For the LGSSM, the filtered kernels are

$$\begin{aligned} \vec{\Psi}_t^{(1)}(x_t | x_{t-1}) &= p(x_t | x_{t-1}, y_t, \theta) \\ &\propto \mathcal{N}(x_t | \phi x_{t-1}, \sigma^2) \cdot \mathcal{N}(y_t | x_t, \tau^2), \\ \vec{\Psi}_t^{(1)}(x_t | x_{t+1}) &= p(x_t | x_{t+1}, y_t, \theta) \\ &\propto \mathcal{N}(x_t | \phi x_{t+1}, \sigma^2) \cdot \mathcal{N}(y_t | x_t, \tau^2). \end{aligned} \quad (\text{A.27})$$

Therefore,

$$\begin{aligned} \vec{\Psi}_t^{(1)}(x_t | x_{t-1}) &= \mathcal{N}\left(x_t \mid \frac{\sigma^2 y_t + \phi \tau^2 x_{t-1}}{\sigma^2 + \tau^2}, \frac{\sigma^2 \tau^2}{\sigma^2 + \tau^2}\right), \\ \vec{\Psi}_t^{(1)}(x_t | x_{t+1}) &= \mathcal{N}\left(x_t \mid \frac{\sigma^2 y_t + \phi \tau^2 x_{t+1}}{\sigma^2 + \tau^2}, \frac{\sigma^2 \tau^2}{\sigma^2 + \tau^2}\right). \end{aligned} \quad (\text{A.28})$$

The associated random mapping are,

$$\begin{aligned} \vec{\psi}_t^{(1)}(x_t | x_{t-1}) &= \frac{\sigma^2 y_t}{\sigma^2 + \tau^2} + \frac{\phi \tau^2}{\sigma^2 + \tau^2} \cdot x_{t-1} + \vec{z}_t, \\ \vec{\psi}_t^{(1)}(x_t | x_{t+1}) &= \frac{\sigma^2 y_t}{\sigma^2 + \tau^2} + \frac{\phi \tau^2}{\sigma^2 + \tau^2} \cdot x_{t+1} + \vec{z}_t, \end{aligned} \quad (\text{A.29})$$

where \vec{z}_t and \tilde{z}_t are $\mathcal{N}\left(0, \frac{\sigma^2 \tau^2}{\sigma^2 + \tau^2}\right)$ random variables.

Since these maps are linear, we have $\|\vec{\Psi}_t^{(1)}\|_{Lip} = \|\tilde{\Psi}_t^{(1)}\|_{Lip} = |\phi| \cdot \frac{\tau^2}{\sigma^2 + \tau^2}$. Applying Theorem 3, we obtain

$$L_\theta \leq \max_t \{\|\vec{\Psi}_t^{(1)}\|, \|\tilde{\Psi}_t^{(1)}\|\} = |\phi| \cdot (1 + \sigma^2/\tau^2)^{-1}. \quad (\text{A.30})$$

Therefore $L_\theta < 1$ whenever $|\phi| < 1 + \sigma^2/\tau^2$.

A.4.2 Contraction Bound for SVM

We assume the prior $\nu(x_0\theta) = \mathcal{N}(0, \sigma^2/(1 - \phi^2))$. For the SVM, the prior kernels are,

$$\begin{aligned} \vec{\Psi}_t^{(0)}(x_t | x_{t-1}) &= p(x_t | x_{t-1}, \theta) \propto \mathcal{N}(x_t | \phi x_{t-1}, \sigma^2), \\ \tilde{\Psi}_t^{(0)}(x_t | x_{t+1}) &= p(x_t | x_{t+1}, \theta) \propto \mathcal{N}(x_t | \phi x_{t+1}, \sigma^2). \end{aligned} \quad (\text{A.31})$$

The associated random mapping are

$$\begin{aligned} \vec{\psi}_t^{(0)}(x_t | x_{t-1}) &= \phi \cdot x_{t-1} + \mathcal{N}(0, \sigma^2), \\ \tilde{\psi}_t^{(0)}(x_t | x_{t+1}) &= \phi \cdot x_{t+1} + \mathcal{N}(0, \sigma^2). \end{aligned} \quad (\text{A.32})$$

Applying Theorem 3, we obtain $L_\theta \leq |\phi|$.

B Model Details Supplement

B.1 LGSSM

The LGSSM in this paper is given by

$$\begin{aligned} X_t | (X_{t-1} = x_{t-1}), \theta &\sim \mathcal{N}(x_t | \phi x_{t-1}, \sigma^2), \\ Y_t | (X_t = x_t), \theta &\sim \mathcal{N}(y_t | x_t, \tau^2), \end{aligned} \quad (\text{B.1})$$

with parameters $\theta = (\phi, \sigma, \tau)$.

When applying the particle filter, Algorithm 1, to the LGSSM, we consider two proposal densities $q(\cdot | \cdot)$:

- The prior (transition) kernel

$$X_t | (X_{t-1} = x_{t-1}), \theta \sim \mathcal{N}(x_t | \phi x_{t-1}, \sigma^2), \quad (\text{B.2})$$

where the weight update, Eq. (3), is

$$w_t^{(i)} \propto \frac{1}{\sqrt{2\pi\tau^2}} \exp\left(\frac{-(y_t - x_t^{(i)})^2}{2\tau^2}\right). \quad (\text{B.3})$$

- The ‘optimal instrumental kernel’

$$\begin{aligned} X_t | (X_{t-1} = x_{t-1}, Y_t = y_t), \theta &\sim \mathcal{N}(x_t | \phi x_{t-1} + \sigma^2 y_t, \sigma^2 \tau^2), \\ &\sim \mathcal{N}\left(x_t \mid \frac{\tau^2 \phi x_{t-1} + \sigma^2 y_t}{\sigma^2 + \tau^2}, \frac{\sigma^2 \tau^2}{\sigma^2 + \tau^2}\right), \end{aligned} \quad (\text{B.4})$$

where the weight update, Eq. (3), is

$$w_t^{(i)} \propto \frac{1}{\sqrt{2\pi(\sigma^2 + \tau^2)}} \exp\left(\frac{-(y_t - \phi x_{t-1}^{(a_i)})^2}{2(\sigma^2 + \tau^2)}\right). \quad (\text{B.5})$$

In our experiments with the LGSSM, we use the optimal instrumental kernel.

For this model, the (elementwise) complete data log-likelihood is

$$\begin{aligned} \log p(y_t, x_t | x_{t-1}, \theta) &= -\log(2\pi) - \log(\sigma) \\ &\quad - \frac{(x_t - \phi x_{t-1})^2}{2\sigma^2} - \log(\tau) - \frac{(y_t - x_t)^2}{2\tau^2}. \end{aligned} \quad (\text{B.6})$$

The gradient of the complete data loglikelihood is then,

$$\begin{aligned} \nabla_\phi \log p(y_t, x_t | x_{t-1}, \theta) &= \frac{(x_t - \phi x_{t-1}) \cdot x_{t-1}}{\sigma^2}, \\ \nabla_\sigma \log p(y_t, x_t | x_{t-1}, \theta) &= \frac{(x_t - \phi x_{t-1})^2 - \sigma^2}{\sigma^3}, \\ \nabla_\tau \log p(y_t, x_t | x_{t-1}, \theta) &= \frac{(y_t - x_t)^2 - \tau^2}{\tau^3}. \end{aligned} \quad (\text{B.7})$$

We reparametrize the gradients with σ^{-1} and τ^{-1} to obtain,

$$\begin{aligned} \nabla_{\sigma^{-1}} \log p(y_t, x_t | x_{t-1}, \theta) &= \frac{\sigma^2 - (x_t - \phi x_{t-1})^2}{\sigma}, \\ \nabla_{\tau^{-1}} \log p(y_t, x_t | x_{t-1}, \theta) &= \frac{\tau^2 - (y_t - x_t)^2}{\tau}. \end{aligned} \quad (\text{B.8})$$

To complete the SGMC scheme, the prior distributions of the parameters θ are given as follows:

$$\begin{aligned} \phi &\sim \mathcal{N}(0, 100 \cdot \sigma^2) \\ \sigma^{-1} &\sim \text{Gamma}(1 + 100, (1 + 100)^{-1}) \\ \tau^{-1} &\sim \text{Gamma}(1 + 100, (1 + 100)^{-1}) . \end{aligned} \quad (\text{B.9})$$

The initial parameter values for synthetic experiments were drawn from:

$$\begin{aligned} \phi &\sim \mathcal{N}(0, 1 \cdot \sigma^2) \\ \sigma^{-1} &\sim \text{Gamma}(2, 0.5) \\ \tau^{-1} &\sim \text{Gamma}(2, 0.5) . \end{aligned} \quad (\text{B.10})$$

B.2 SVM

The SVM in this paper is given by,

$$\begin{aligned} X_t | (X_{t-1} = x_{t-1}), \theta &\sim \mathcal{N}(x_t | \phi x_{t-1}, \sigma^2), \\ Y_t | (X_t = x_t), \theta &\sim \mathcal{N}(y_t | 0, \exp(x_t)\tau^2), \end{aligned} \quad (\text{B.11})$$

with parameters $\theta = (\phi, \sigma, \tau)$. In this model, the observations, $y_{1:T}$, represent the logarithm of the daily difference in the exchange rate and X is the unobserved volatility. We assume that the volatility process is stationary (such that $0 < \phi < 1$), where ϕ is the persistence in volatility and τ is the instantaneous volatility.

For the particle filter, we use the prior kernel as the proposal density q

$$X_t | (X_{t-1} = x_{t-1}), \theta \sim \mathcal{N}(x_t | \phi x_{t-1}, \sigma^2), \quad (\text{B.12})$$

with weight update

$$w_t^{(i)} \propto \frac{1}{\sqrt{2\pi\tau^2}} \exp\left(\frac{-y_t^2}{2\exp(x_t^{(i)})\tau^2}\right). \quad (\text{B.13})$$

The elementwise complete data loglikelihood is

$$\begin{aligned} \log p(y_t, x_t | x_{t-1}, \theta) &= -\log(2\pi) - \log(\sigma) - \log(\tau) \\ &\quad - \frac{(x_t - \phi x_{t-1})^2}{2\sigma^2} - 0.5x_t - \frac{(y_t)^2}{2\exp(x_t)\tau^2}. \end{aligned} \quad (\text{B.14})$$

The gradient of the complete data loglikelihood is then,

$$\begin{aligned} \nabla_\phi \log p(y_t, x_t | x_{t-1}, \theta) &= \frac{(x_t - \phi x_{t-1}) \cdot x_{t-1}}{\sigma^2}, \\ \nabla_\sigma \log p(y_t, x_t | x_{t-1}, \theta) &= \frac{(x_t - \phi x_{t-1})^2 - \sigma^2}{\sigma^3}, \\ \nabla_\tau \log p(y_t, x_t | x_{t-1}, \theta) &= \frac{y_t^2 / \exp(x_t) - \tau^2}{\tau^3}. \end{aligned} \quad (\text{B.15})$$

We parametrize with σ^{-1} and τ^{-1} to obtain,

$$\begin{aligned} \nabla_{\sigma^{-1}} \log p(y_t, x_t | x_{t-1}, \theta) &= \frac{\sigma^2 - (x_t - \phi x_{t-1})^2}{\sigma}, \\ \nabla_{\tau^{-1}} \log p(y_t, x_t | x_{t-1}, \theta) &= \frac{\tau^2 - y_t^2 / \exp(x_t)}{\tau}. \end{aligned} \quad (\text{B.16})$$

The prior distributions and initializations of the parameters θ are taken to be the same as in the LGSSM case.

B.3 GARCH Model

The GARCH(1,1) model in this paper is given by,

$$\begin{aligned} X_t | (X_{t-1} = x_{t-1}), \sigma_t^2, \theta &\sim \mathcal{N}(x_t | 0, \sigma_t^2), \\ \sigma_t^2(x_{t-1}, \sigma_{t-1}^2, \theta) &= \alpha + \beta x_{t-1}^2 + \gamma \sigma_{t-1}^2, \\ Y_t | (X_t = x_t), \theta &\sim \mathcal{N}(y_t | x_t, \tau^2), \end{aligned} \quad (\text{B.17})$$

where parameters are $\theta = (\log \mu, \text{logit } \phi, \text{logit } \lambda, \tau)$ for $\alpha = \mu(1 - \phi)$, $\beta = \phi\lambda$, $\gamma = \phi(1 - \lambda)$. Note that $\sigma_t^2 = \mu(1 - \phi) + \phi(\lambda x_{t-1}^2 + (1 - \lambda)\sigma_{t-1}^2)$.

We consider two proposal densities $q(\cdot | \cdot)$ for the GARCH model:

- The prior kernel

$$\begin{aligned} \left[\begin{array}{c} X_t \\ \sigma_t^2 \end{array} \right] | \left[\begin{array}{c} X_{t-1} = x_{t-1} \\ \sigma_{t-1}^2 \end{array} \right], \theta \\ \sim \left[\begin{array}{c} \mathcal{N}(x_t | 0, \alpha + \beta x_{t-1}^2 + \gamma \sigma_{t-1}^2) \\ \delta(\sigma_t^2 | \alpha + \beta x_{t-1}^2 + \gamma \sigma_{t-1}^2) \end{array} \right]. \end{aligned} \quad (\text{B.18})$$

where the weight update, Eq. (3), is

$$w_t^{(i)} \propto \frac{1}{\sqrt{2\pi\tau^2}} \exp\left(\frac{-(y_t - x_t^{(i)})^2}{2\tau^2}\right). \quad (\text{B.19})$$

- The optimal instrumental kernel

$$\begin{aligned} \left[\begin{array}{c} X_t \\ \sigma_t^2 \end{array} \right] | \left[\begin{array}{c} X_{t-1} = x_{t-1} \\ \sigma_{t-1}^2 \end{array} \right], (Y_t = y_t), \theta \\ \sim \left[\begin{array}{c} \mathcal{N}(x_t | \sigma_t^2 y_t / (\sigma_t^2 + \tau^2), \sigma_t^2 \tau^2 / (\sigma_t^2 + \tau^2)) \\ \delta(\sigma_t^2 | \alpha + \beta x_{t-1}^2 + \gamma \sigma_{t-1}^2) \end{array} \right]. \end{aligned} \quad (\text{B.20})$$

where the weight update, Eq. (3), is

$$w_t^{(i)} \propto \frac{1}{\sqrt{2\pi((\sigma_t^{(i)})^2 + \tau^2)}} \exp\left(\frac{-y_t^2}{2((\sigma_t^{(i)})^2 + \tau^2)}\right). \quad (\text{B.21})$$

In our experiments with the GARCH model, we use the optimal instrumental kernel.

The elementwise complete data loglikelihood is

$$\begin{aligned} \log p(y_t, x_t, \sigma_t^2 | x_{t-1}, \sigma_{t-1}^2, \theta) &= \\ &\quad - \frac{\log(2\pi) + \log(\alpha + \beta x_{t-1}^2 + \gamma \sigma_{t-1}^2)}{2} \\ &\quad - \frac{x_t^2}{2(\alpha + \beta x_{t-1}^2 + \gamma \sigma_{t-1}^2)} \\ &\quad - 0.5 \log(2\pi) - \log(\tau) - \frac{(y_t - x_t)^2}{2\tau^2}. \end{aligned} \quad (\text{B.22})$$

Let $\mathcal{L}_t = \log p(y_t, x_t, \sigma_t^2 | x_{t-1}, \sigma_{t-1}^2, \theta)$ and set $C_t = \frac{x_t^2 - \sigma_t^2}{2\sigma_t^4}$. Then the gradient of the complete data loglikelihood $\nabla \mathcal{L}_t$ is

$$\begin{aligned} \nabla_{\tau} \mathcal{L}_t &= \frac{(y_t - x_t)^2 - \tau^2}{\tau^3}, \\ \nabla_{\log \mu} \mathcal{L}_t &= C_t \cdot (1 - \phi) \cdot \mu, \\ \nabla_{\text{logit } \phi} \mathcal{L}_t &= C_t \cdot (\lambda x_{t-1}^2 + (1 - \lambda)\sigma_{t-1}^2 - \mu) \cdot \phi(1 - \phi), \\ \nabla_{\text{logit } \lambda} \mathcal{L}_t &= C_t \cdot (\phi x_{t-1}^2 - \phi \sigma_{t-1}^2) \cdot \lambda(1 - \lambda). \end{aligned} \quad (\text{B.23})$$

The SGMC scheme is completed by setting the prior distributions for the parameters as follows: $(\phi + 1)/2 \sim \text{Beta}(10, 1.5)$, $\mu \sim \text{Uniform}(0, 2)$, $(\lambda + 1)/2 \sim \text{Beta}(20, 1.5)$ and $\tau^2 \sim \mathcal{IG}(2, 0.5)$.

C Additional Experiment

We first present the stochastic gradient bias when using PaRIS with the LGSSM data. We then present additional SGLD results on synthetic data for the LGSSM in higher dimensions, the SVM and the GARCH models. We finally present some additional details for the SGLD experiment on the EUR-US exchange rate data.

C.1 Gradient Bias with PaRIS

Figure C.1 compares the stochastic gradient bias of the naive PF with PaRIS on the LGSSM data in Section 5.2.

From Figure C.1 (top) and (bottom-left), we see that the naive PF (blue or solid line) performs similarly to PaRIS (red or dashed line) as N varies. However, Figure C.1 (bottom-right) shows that the naive PF is about 10 times faster per iteration than PaRIS.

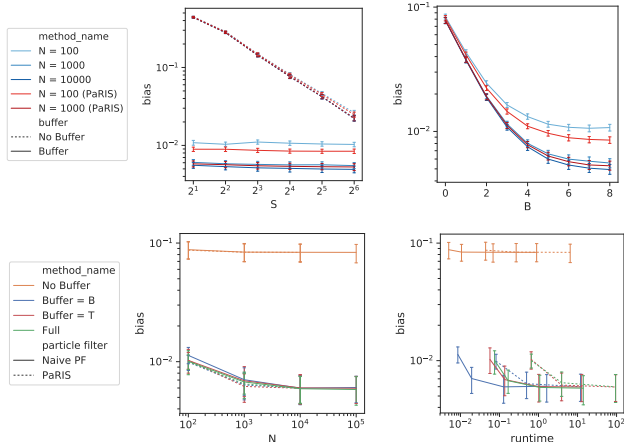


Figure C.1: Stochastic gradient bias varying B, S, N for the naive PF and PaRIS on the LGSSM data. (Top-left) bias vs S , (top-right) bias vs B , (bottom-left) bias vs N , (bottom-right) bias vs runtime in seconds. Error bars are 95% CI over 1000 replications.

C.2 SGLD on Synthetic Data

C.2.1 Additional MSE Figures for LGSSM

Figure C.2 presents extra MSE plots for the parameters not presented in the main paper. Tables C.1 and C.2 present the full KSD results for each variable.

C.2.2 Higher Dimensional LGSSM

We generate synthetic LGSSM data for $X_t, Y_t \in \mathbb{R}^d$ using $\phi = 0.9 \cdot \mathbb{I}_d$, $\sigma = 0.7 \cdot \mathbb{I}_d$, and $\tau = \mathbb{I}_d$ for dimensions $d \in \{5, 10\}$. Figure C.3 presents the trace plot metrics for $d = 5$ and for $d = 10$. Table C.3 presents the KSD tables for both.

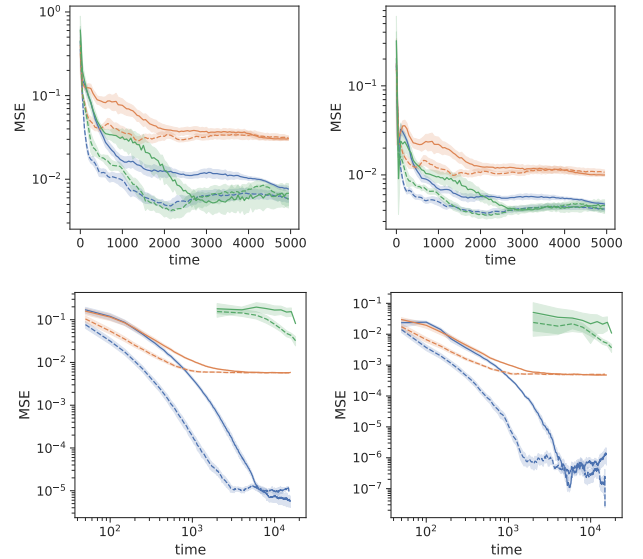


Figure C.2: Additional metrics for SGLD on LGSSM: (left) MSE of σ , (right) MSE of τ , (top) $T = 10^3$, (bottom) $T = 10^6$

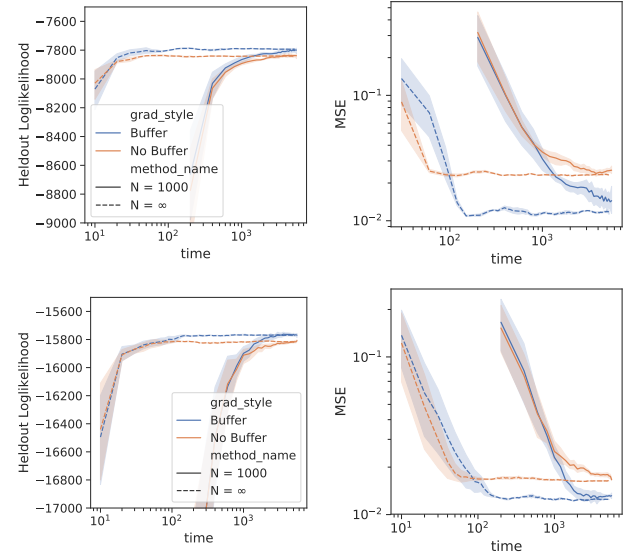


Figure C.3: SGLD Results for LGSSM $X \in \mathbb{R}^{10}$: (left) heldout loglikelihood, (right) MSE of ϕ .

We find that the Kalman filter $N = \infty$ is able to much more rapidly mix compared to the particle filter with $N = 1000$. This is both due to the increased particle filter variance in higher dimensions and the longer computation required for sampling particles in higher dimensions. However in both cases, we again see that buffering is necessary to avoid bias.

Table C.1: KSD results for Synthetic LGSSM with $T = 10^3$

S	B	METHOD	$\log_{10}\text{KSD}$			TOTAL
			ϕ	σ	τ	
10^3	-	GIBBS	0.09 (0.25)	-0.02 (0.01)	-0.16 (0.48)	0.51 (0.13)
		KF	0.01 (0.57)	0.07 (0.09)	0.20 (0.28)	0.64 (0.17)
		PF	0.38 (0.26)	0.10 (0.16)	0.44 (0.19)	0.85 (0.08)
40	0	KF	1.53 (0.03)	-0.08 (0.07)	-0.04 (0.16)	1.55 (0.03)
		PF	1.55 (0.03)	-0.04 (0.13)	0.10 (0.26)	1.58 (0.03)
40	10	KF	0.18 (0.27)	0.02 (0.07)	0.04 (0.44)	0.61 (0.21)
		PF	0.27 (0.46)	0.09 (0.13)	-0.11 (0.53)	0.68 (0.25)

Table C.2: KSD results for Synthetic LGSSM with $T = 10^6$

S	B	METHOD	$\log_{10}\text{KSD}$			TOTAL
			ϕ	σ	τ	
10^6	-	GIBBS	3.91 (0.80)	3.43 (1.07)	3.52 (0.73)	4.23 (0.74)
		KF	4.51 (0.48)	4.21 (0.50)	3.65 (0.55)	4.85 (0.36)
		PF	4.77 (0.39)	4.11 (0.57)	3.55 (0.95)	4.92 (0.40)
40	0	KF	4.64 (0.14)	3.25 (0.21)	2.83 (0.61)	4.68 (0.11)
		PF	4.64 (0.13)	3.19 (0.35)	3.12 (0.45)	4.68 (0.10)
40	10	KF	3.04 (0.39)	1.57 (0.50)	2.68 (0.20)	3.25 (0.29)
		PF	3.26 (0.17)	1.70 (0.38)	2.87 (0.33)	3.43 (0.19)

Table C.3: KSD results for Synthetic LGSSM in higher dimensions

DIM	GRAD EST.	N	$\log_{10}\text{KSD}$			
			ϕ	σ	τ	TOTAL
5	NO BUFFER	1000	1.78 (0.04)	1.97 (0.26)	1.44 (0.45)	2.28 (0.20)
		∞	1.74 (0.01)	2.09 (0.02)	1.64 (0.02)	2.35 (0.01)
	BUFFER	1000	1.18 (0.17)	1.74 (0.25)	1.44 (0.03)	2.01 (0.13)
		∞	0.84 (0.03)	1.97 (0.03)	1.40 (0.05)	2.10 (0.03)
10	NO BUFFER	1000	1.84 (0.01)	2.40 (0.06)	2.26 (0.13)	2.71 (0.06)
		∞	1.79 (0.01)	2.13 (0.04)	2.12 (0.01)	2.52 (0.02)
	BUFFER	1000	1.60 (0.13)	2.37 (0.04)	2.20 (0.04)	2.64 (0.04)
		∞	1.04 (0.06)	2.08 (0.04)	2.07 (0.01)	2.39 (0.02)

C.2.3 SVM

Figure C.4 presents the trace plot metrics for SGLD on the synthetic SVM data $T = 1000$ and Table C.4 presents the KSD for each sampled chain.

We find that buffering performs best (as measured by KSD). From Figure C.4 we see that not buffering leads to bias, while the full sequence method is nosier (fewer larger steps) compared to the buffer method.

C.2.4 GARCH

Figure C.5 presents the trace plot metrics for SGLD on the synthetic GARCH data $T = 1000$ and Table C.5 presents the KSD for each sampled chain.

We again find that buffering performs best (as measured by KSD). From Figure C.5 we see that not buffering leads to bias in sampling μ and λ . The full sequence method encounters high particle error and therefore

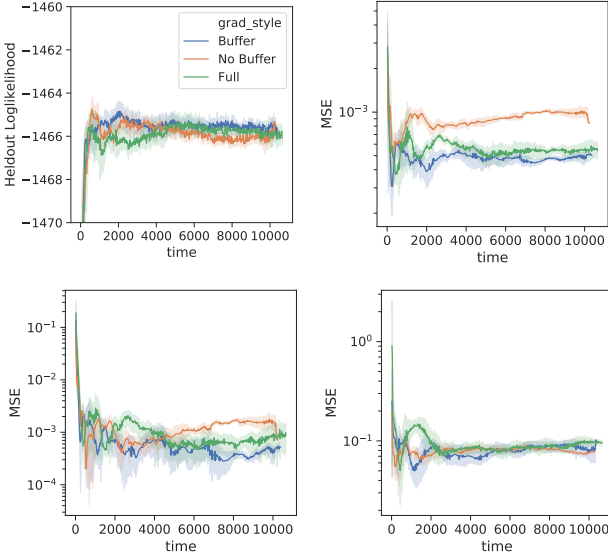


Figure C.4: SGLD results for synthetic SVM data: (top-left) heldout loglikelihood, (top-right) MSE of ϕ , (bottom-left) MSE of σ , (bottom-right) MSE of τ .

requires a much longer runtime with a much smaller stepsize to reduce bias.

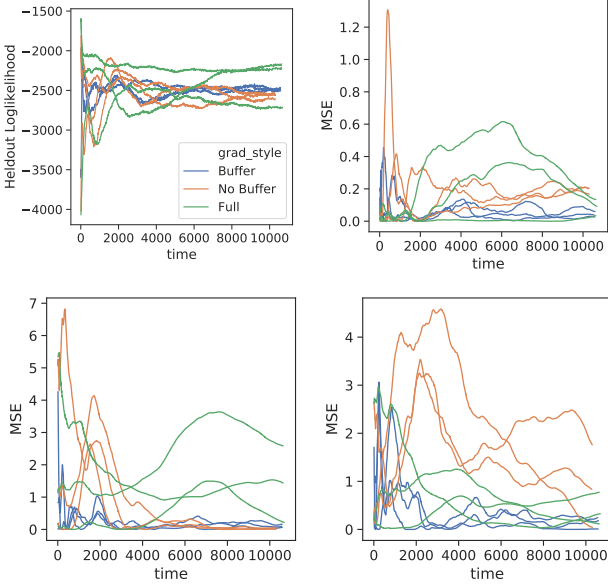


Figure C.5: SGLD results for synthetic SVM data: (top-left) heldout loglikelihood, (top-right) MSE of $\log(\mu)$, (bottom-left) MSE of $\text{logit } \phi$, (bottom-right) MSE of $\text{logit } \lambda$.

C.3 SGLD on Exchange Rate

The EUR-US exchange rate data was fuled from the <https://www.finam.ru> website for the time period of November 2017 to October 2018 at the minute resolution. The *demeaned log-returns* are calculated by taking the difference of the log-closing price (at each minute) and removing the mean, as done in the `stochvol` package in R (Kastner, 2016)

$$\tilde{y}_t = \log(y_t/y_{t-1}) - \frac{1}{T} \sum_{t'} \log(y_{t'}/y_{t'-1}) . \quad (\text{C.1})$$

The data is plotted in Figure C.6.

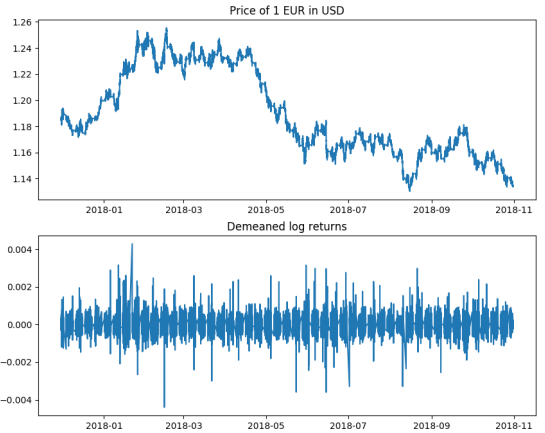


Figure C.6: EUR-US Exchange Rate Data (top) raw data (bottom) demeaned log-returns

C.3.1 SVM

For the SVM, we initialized each chain at $\phi = 0.9$, $\sigma = 1.73$ and $\tau = 0.1$ for all SGLD methods. The full KSD results are presented in Table C.6.

C.3.2 GARCH

For the GARCH model, we initialized each chain at $\log \mu = -0.4$, $\text{logit } \phi = 1.7$, $\text{logit } \lambda = 2.7$ and $\tau = 0.1$ for all SGLD methods. The full KSD results are presented in Table C.7.

Table C.4: KSD results for Synthetic SVM

		$\log_{10}\text{KSD}$		
GRAD EST.		ϕ	σ	τ
				TOTAL
FULL		0.68 (0.28)	0.38 (0.40)	0.44 (0.54)
NO BUFFER		1.49 (0.05)	-0.01 (0.23)	0.09 (0.35)
BUFFER		0.35 (0.33)	0.23 (0.29)	0.21 (0.40)
				0.81 (0.22)

Table C.5: KSD results for Synthetic GARCH

		$\log_{10}\text{KSD}$			
GRAD EST.		$\log \mu$	logit λ	logit ϕ	τ
					TOTAL
FULL		0.29 (0.59)	0.04 (0.03)	0.18 (0.34)	0.55 (0.11)
NO BUFFER		0.07 (0.08)	-0.38 (0.09)	-0.15 (0.10)	0.56 (0.10)
BUFFER		-0.27 (0.24)	-0.72 (0.19)	-0.69 (0.17)	0.12 (0.19)
					0.39 (0.09)

Table C.6: KSD results for SVM on exchange rate data.

		$\log_{10}\text{KSD}$			
GRAD EST.		ϕ	σ	τ	TOTAL
FULL		3.63 (0.30)	3.76 (0.07)	1.46 (0.38)	4.03 (0.14)
WEEKLY		3.86 (0.08)	2.18 (0.28)	0.67 (0.39)	3.87 (0.08)
NO BUFFER		4.48 (0.01)	1.84 (0.15)	1.21 (0.14)	4.48 (0.01)
BUFFER		3.53 (0.11)	2.32 (0.13)	1.23 (0.05)	3.56 (0.10)

Table C.7: KSD results for GARCH on exchange rate data.

		$\log_{10}\text{KSD}$			
GRAD EST.		$\log \mu$	logit λ	logit ϕ	τ
					TOTAL
FULL		2.18 (0.67)	2.18 (0.07)	2.19 (0.61)	2.07 (0.06)
WEEKLY		2.17 (0.51)	2.21 (0.03)	2.31 (0.29)	1.85 (0.19)
NO BUFFER		1.76 (0.06)	1.43 (0.46)	1.31 (0.09)	1.58 (0.08)
BUFFER		1.76 (0.03)	2.01 (0.08)	1.11 (0.07)	2.09 (0.09)
					2.19 (0.05)